Dark matter and electroweak symmetry breaking in models with warped extra dimensions

Giuliano Panico,[1,2] Eduardo Pontón,[3] José Santiago,[4,5] and Marco Serone[1]

[1]*ISAS-SISSA and INFN, Via Beirut 2-4, I-34013 Trieste, Italy*

[2]*Physikalisches Institut der Universität Bonn, Nussallee 12, 53115 Bonn, Germany*

[3]*Department of Physics, Columbia University, 538 West 120th Street, New York, New York 10027, USA*

[4]*FERMILAB, P.O. Box 500, Batavia, Illinois 60510, USA*

[5]*Institute for Theoretical Physics, ETH, CH-8093, Zürich, Switzerland*

(Received 5 February 2008; published 16 June 2008)

We show that a discrete *exchange* symmetry can give rise to realistic dark matter candidates in models with warped extra dimensions. We show how to realize our construction in a variety of models with warped extra dimensions and study in detail a realistic model of gauge-Higgs unification/composite Higgs in which the observed amount of dark matter is naturally reproduced. In this model, a realistic pattern of electroweak symmetry breaking typically occurs in a region of parameter space in which the fit to the electroweak precision observables improves, the Higgs is heavier than the experimental bound and new light quark resonances are predicted. We also quantify the fine-tuning of such scenarios, and discuss in which sense gauge-Higgs unification models result in a natural theory of electroweak symmetry breaking.

DOI: 10.1103/PhysRevD.77.115012 PACS numbers: 12.60.Cn, 95.35.+d

I. INTRODUCTION

Models with warped extra dimensions [1] have arisen in the last few years as strong candidates for a natural theory of electroweak symmetry breaking (EWSB). The original solution to the hierarchy problem has been supplemented by the addition of a natural flavor structure [2], a custodial symmetry to protect the T parameter [3] and the $Z\bar{b}_L b_L$ coupling [4], and the realization of the Higgs as the pseudo-Goldstone boson of a broken global symmetry [5–7]. These developments have produced calculable models that successfully address most of the mysteries related to the electroweak (EW) scale.

On the other hand, dark matter (DM), that is often considered one of the strongest—albeit indirect—hints of physics beyond the standard model (SM), has so far lacked a generic implementation in models with warped extra dimensions. The main reason is the inherent asymmetry in warped backgrounds, that do not possess a natural Kaluza-Klein (KK) parity as the one present in universal extra dimensions (UEDs) [8].

In this article we explore a generic procedure to introduce an exact discrete exchange symmetry that results in new stable states, without introducing new parameters. This is done via a doubling of part of the field content. The exchange symmetry we advocate has been first introduced in [9] (where it was dubbed ''mirror symmetry'') and [10] to alleviate the fine-tuning and to get a viable DM candidate in gauge-Higgs unification (GHU) models in flat space. As already anticipated in [9], it can be extended-straightforwardly to warped models. Given a bulk field ϕ, satisfying certain boundary conditions (b.c.), the procedure consists of replacing ϕ by a pair of fields ϕ_1 and ϕ_2 and imposing the symmetry $\phi_1 \leftrightarrow \phi_2$.[1] The even linear combination $\phi_+ \equiv (\phi_1 + \phi_2)/\sqrt{2}$ is identified with the original field (in particular, it inherits the b.c. obeyed by ϕ, as well as its couplings). The couplings of the orthogonal combination $\phi_- \equiv (\phi_1 - \phi_2)/\sqrt{2}$ are determined by those of ϕ_+. Under the exchange symmetry one has $\phi_\pm \to \pm\phi_\pm$, so that one can assign a multiplicative charge $+1$ to ϕ_+ and -1 to ϕ_-. Provided the discrete exchange symmetry is an exact symmetry at the quantum level, the lightest KK resonance among all $\mathbf{Z}_2$-odd states in the model is absolutely stable, and will be referred to as the LOP (lightest odd particle). We argue that the above symmetry is indeed exact, by showing that possible 5D Chern-Simons (CS) terms, in general needed to restore gauge invariance in 5D theories, do not violate it [12].

The choice of which fields to double must be guided by phenomenological considerations. For example, DM direct and indirect searches impose stringent constraints on the possible couplings of the DM candidate to SM fields. It is therefore natural to look for charge and color neutral fields that can lead to viable DM candidates. In fact, the models we will consider always contain $U(1)$ factors, and it will be natural for the DM candidate to be a $U(1)$ massive gauge field X_-. This is similar to the 5D UED case and the GHU model of [10] in flat space, in which the DM can be identified with the first KK mode of the hypercharge gauge field. If the LOP were the only $\mathbf{Z}_2$-odd particle, it would couple to SM fields only via nonrenormalizable interactions. For the typical scales involved, its annihilation rate would then be extremely small, and the resulting thermal

[1]A similar discrete symmetry has recently been used in [11] to get a DM candidate in the context of little Higgs theories.

relic density unacceptably large. Hence, it is necessary in general to apply the previously described ''doubling'' construction to additional fields, making sure that X_- remains the lightest among the $\mathbf{Z}_2$-odd particles. We can choose b.c. for the LOP so that it has a mass about an order of magnitude smaller than the mass of the first $\mathbf{Z}_2$-even gauge resonances. Thus, our DM candidate has typically sub-TeV masses, which, as we will see, can range from $\sim$100 GeV in Higgsless models up to $\sim$700 GeV in Randall-Sundrum (RS) models. Together with its mass, the coupling of the LOP to SM matter is the other crucial parameter governing its relic density. In all the cases we will consider, the $U(1)$ symmetry is related to the SM $U(1)_Y$ symmetry, with a coupling constant of electroweak size, and the $\mathbf{Z}_2$-odd fields will consist of X_- and a subset of fermion fields, typically associated with the top or bottom quarks. It is clear that our DM candidate is a weakly interacting massive particle with approximately the correct mass and couplings to give rise to the observed DM relic density in the Universe.

The construction outlined above turns out to be particularly natural in the specific class of GHU scenarios in warped space.[2] In this case, the additional set of fields introduced by our procedure is not only minimal, but is also singled out by the role the doubled sector plays in generating the EW scale dynamically. Although it is not easy to use the discrete symmetry to protect EW observables from large tree-level corrections, as in R-parity-preserving supersymmetric scenarios, little Higgs theories with T parity, or UED with KK parity, we will see that the physics of EWSB in the GHU model with the discrete symmetry naturally leads to a region in parameter space where the constraints due to precision measurements are relaxed. Furthermore, this same region of parameter space, in which coannihilation effects can be relevant, predicts a dark matter abundance in accord with observation. Thus, the DM sector is tightly connected to the physics of EWSB, and plays an indirect role in leading to agreement with precision constraints.[3] Also, the model is rather predictive, with several fermionic resonances nearly degenerate with the DM particle that should lead to an exciting collider phenomenology.

We also consider some nonperturbative effects—the formation of bound states and the effect of QCD Coulomb-like forces—which might invalidate the usual perturbative computation of the relic density. We argue that the problem of the formation of bound states does not occur and that the effect of Coulomb-like forces on the perturbative cross sections is negligible.

We also discuss in some detail the degree of fine-tuning involved in the EWSB pattern, and compare to supersymmetric extensions of the standard model. It turns out that in the GHU framework (with or without DM) the fine-tuning is somewhat worse than expected by naive considerations. We point out, however, that here the fine-tuning seems to be associated with accommodating a top mass of order the EW scale, rather than with an intrinsic tension in the Higgs sector. When restricted to the region of parameter space with a fixed top mass, the low-energy properties of the model turn out to be essentially insensitive to the microscopic parameters of the model, and therefore to the detailed properties of the new physics, which is a very interesting feature.

Although we find the application of our construction to the GHU framework particularly appealing, we stress that it is of more general applicability. We also briefly discuss the implementation of the discrete exchange symmetry in two other models with warped extra dimensions: the simplest RS model with the SM fermions and gauge bosons in the bulk, and a Higgsless model. Hence, our construction leads to viable DM candidates in a variety of scenarios, without the introduction of new parameters.

The organization of the paper is as follows. In Sec. II we review the generic properties of the exchange $\mathbf{Z}_2$ symmetry that gives rise to a dark matter candidate. In Sec. III we discuss in detail its implementation in a model of GHU. In particular, we study the interplay between EWSB, the EW constraints and the DM relic abundance, the (ir)relevance of the above-mentioned nonperturbative effects, and discuss the fine-tuning. In Sec. IV we describe the implementation of the discrete exchange symmetry in other models. Section V is devoted to particular details of DM collider phenomenology and DM direct detection in our construction. We comment on the issue of anomalies in Sec. VI, and conclude in Sec. VII. We relegate some technical details to Appendixes A, B, and C.

II. EXCHANGE $\mathbf{Z}_2$ SYMMETRY AND STABLE PARTICLES

The simplest way to get a stable massive particle X_- beyond the SM spectrum is obtained by introducing a discrete $\mathbf{Z}_2$ symmetry under which all SM particles are even, with X_- the lightest $\mathbf{Z}_2$-odd particle. For example, viable DM candidates in promising models of new physics, such as supersymmetric (SUSY) or little Higgs models, are stable due to $\mathbf{Z}_2$ symmetries (R and T parity [15], respectively). In the context of extra-dimensional theories, a geometric $\mathbf{Z}_2$ symmetry called KK parity leads to viable DM particles in 5D [16] and 6D [17] UED scenarios. Most extradimensional models which aim at stabilizing the electroweak scale are based on warped compactifications of the

[2]It is known that such models can also be seen, thanks to the anti-de Sitter/conformal field theory dictionary [13], as strongly coupled 4D composite Higgs models. However, since calculability requires the 5D picture, we will mostly use the 5D language, adopting only occasionally the 4D dual language.

[3]See [14] for a model in which EWSB and DM are related. In this reference, however, the hierarchy problem is not addressed.

Randall-Sundrum type [1], with bulk gauge and fermion fields [2], where KK parity cannot be trivially imposed.[4] We are therefore motivated to look for other discrete symmetries that could lead to DM candidates in such warped scenarios.

From a model-building point of view, it is always possible to impose a discrete symmetry *ad hoc* for the only purpose of getting a stable particle, possibly with the correct properties to account for the observed DM density. Such constructions become far more interesting if the DM sector is tightly connected with other sectors of a given theory, in such a way that it leads to additional testable predictions and/or no new parameters are introduced. The $\mathbf{Z}_2$ exchange symmetry we consider belongs to this class, since no new parameters are added. Furthermore, in the particular class of GHU models, which will be considered in detail in the next section, it can also improve the EWSB pattern and lead to better agreement with electroweak constraints.

Consider a model with warped extra dimensions and a bulk gauge symmetry that includes a $U(1)$ factor $\mathcal{G} \times U(1)_X$. Our construction introduces a discrete symmetry that acts on the $U(1)_X$ factor and leads to a stable spin-1 particle. The group $\mathcal{G}$ does not play any role in our construction (it will be neutral under the discrete symmetry) and we will not discuss it any further. The first step is to double the $U(1)_X$ field: $U(1)_X \to U(1)_{X_1} \times U(1)_{X_2}$. The original $U(1)_X$ gauge boson is identified with the symmetric combination $X_+ \equiv (X_1 + X_2)/\sqrt{2}$, and the gauge couplings chosen as $g_{X_1} = g_{X_2} = \sqrt{2} g_X$, so that X_+ couples with strength g_X. The antisymmetric combination $X_- \equiv (X_1 - X_2)/\sqrt{2}$ is odd under the $\mathbf{Z}_2$ exchange symmetry under which $X_1 \leftrightarrow X_2$.

As remarked in the introduction, doubling only a $U(1)$ symmetry is not enough to obtain a realistic DM candidate. In order to improve this, we take a subset[5] of the fermionic fields in the model ψ, with $U(1)_X$ charge Q_X, and double them into mirror pairs $\psi \to \psi_{1,2}$, assigning them $U(1)_{X_1} \times U(1)_{X_2}$ charges $(Q_X, 0)$ and $(0, Q_X)$, respectively. Finally, undoubled fermions φ, with charge Q under the original $U(1)_X$ group, are assigned charges $(\frac{1}{2}Q, \frac{1}{2}Q)$, which implies that they couple only to the symmetric combination X_+, with charge Q. Since ψ_1 couples only to X_1, while ψ_2 couples only to X_2, the relevant 5D Lagrangian density is $\mathcal{L} = \mathcal{L}_1 + \mathcal{L}_2$ with

$$e^{-1}\mathcal{L}_i = -\tfrac{1}{4}F_i^2 + \bar{\psi}_i[\mathrm{i}\gamma^M(\mathcal{D}_M + \mathrm{i}Q_X g_{X_i} X_{iM}) - m_i]\psi_i, \quad i = 1, 2, \tag{2.1}$$

where F_i is the field strength of the gauge field X_i with 5D coupling constant g_{X_i}, $\mathcal{D}_M$ is the gravitationally covariant derivative and e is the determinant of the fünfbein associated to the 5D metric

$$ds^2 = e^{-2ky}\eta_{\mu\nu}dx^\mu dx^\nu - dy^2 = \left(\frac{z_{\mathrm{UV}}}{z}\right)^2(\eta_{\mu\nu}dx^\mu dx^\nu - dz^2), \tag{2.2}$$

where, as usual, μ runs over the 4D directions, $0 \le y \le L$, $z_{\mathrm{UV}} \le z \le z_{\mathrm{IR}}$, $z = e^{ky}/k$. In Eq. (2.1), we have not explicitly written terms containing the gauge bosons of the group $\mathcal{G}$ or the undoubled fermions. The exchange symmetry constraints $m_1 = m_2 = m \equiv ck$. Notice that for simplicity we omit a possible mixing term of the form $F_1 F_2$ in Eq. (2.1). Similarly, depending on the b.c. chosen for the $\mathbf{Z}_2$-odd fields, possible boundary terms can appear. We assume here that all these operators can be neglected, so that no new parameters are introduced. In terms of $\pm$ fields, we have

$$\begin{aligned} e^{-1}\mathcal{L} = {} & -\tfrac{1}{4}(F_+^2 + F_-^2) + \bar{\psi}_+(\mathrm{i}\gamma^M\mathcal{D}_M - m)\psi_+ \\ & + \bar{\psi}_-(\mathrm{i}\gamma^M\mathcal{D}_M - m)\psi_- - g_X Q_X \gamma^M(\bar{\psi}_+ X_{+M}\psi_+ \\ & + \bar{\psi}_- X_{+M}\psi_- + \bar{\psi}_+ X_{-M}\psi_- + \bar{\psi}_- X_{-M}\psi_+). \end{aligned} \tag{2.3}$$

Let us now discuss the boundary conditions for the different fields. As explained above, X_+ inherits the b.c. of the original $U(1)_X$ gauge boson (that can in general involve in a nontrivial way the neutral gauge bosons in the group $\mathcal{G}$). The b.c. for the odd combination are taken to be

$$X_{-\mu} = \frac{1}{\sqrt{2}}(X_{1\mu} - X_{2\mu}) \sim (+, -), \tag{2.4}$$

where $+/-$ denote Neumann/Dirichlet b.c., respectively, with the first/second entry in parenthesis referring to the UV/IR boundary (X_{-5} satisfies opposite b.c.). These b.c. allow for UV brane localized kinetic terms characterized by a dimensionful coefficient r_{UV}^- (in the notation of Ref. [22]). The lightest X_- resonance (the LOP) has mass of order

$$m_{X_-} \simeq \sqrt{\frac{2}{k(L + r_{\mathrm{UV}}^-)}}\mu_{\mathrm{IR}} \simeq \sqrt{\frac{2}{kL}}\mu_{\mathrm{IR}}, \tag{2.5}$$

where $\mu_{\mathrm{IR}} = ke^{-kL} = 1/z_{\mathrm{IR}}$ and the second equality holds whenever the localized term is small. This mass is parametrically smaller than the KK scale μ_{IR}. For example, for values of kL that solve the hierarchy problem, m_{X_-} is about a factor of 10 below the mass of other gauge resonances, which are of order $m_{X_+} \simeq 2.5\mu_{\mathrm{IR}}$. Note that $(-, +)$ b.c. for X_- would instead give a larger mass, of order m_{X_+}. It

[4]Reference [18] considered a discrete symmetry to forbid low scale baryon number violation in grand unified models, that also gave rise to a stable DM candidate. See also [19] for a recent attempt to include KK parity in warped space, and [20] for some proposals of DM candidates in composite Higgs models.

[5]Doubling the whole spectrum is unnatural, since fermions with twisted boundary conditions can have exponentially small masses [18,21], giving rise to unacceptable LOPs. In fact, as we will see, requiring X_- to be the LOP constrains $|c| < 1/2$ for the doubled fermions.

would then be hard to identify X_- as the LOP and get the correct relic density with such a choice of b.c., without the introduction of large brane kinetic terms. For these reasons, we do not consider this possibility.

Regarding the doubled fermions, ψ_+ satisfies the boundary conditions of the original fermion. The odd combination ψ_- should obey $(+,-)$ or $(-,+)$ b.c. (for one chirality, opposite for the other one) so that no fermion zero modes are introduced in the $\mathbf{Z}_2$-odd sector of the theory.[6] However, the unbroken $U(1)_-$ symmetry on the UV brane, that mixes the two mirror fermions $\psi_\pm$, requires that the b.c. of ψ_- be equal to that of ψ_+ *on the UV brane*. The mass of the first KK mode of ψ_- strongly depends on c. For $|c| \geq 1/2$, this lightest fermionic KK mode can be lighter than X_-. In the context of warped scenarios that solve the flavor puzzle by fermion localization, this usually means that we can only double the fermions associated with the top and bottom quarks, which have $|c| < 1/2$.

These are the qualitative, model-independent features of our mechanism to endow existing models with a stable particle that can be a DM candidate. In the next section, we apply this construction to a very appealing model of EWSB in warped extra dimensions, studying in detail the pattern of EWSB, EW precision tests and the calculation of the DM relic density. In Sec. IV we will briefly show how this construction can be easily implemented in a variety of models with warped extra dimensions.

III. A RELEVANT CASE: A GHU/COMPOSITE HIGGS MODEL

Models of GHU (see e.g. [23] for a brief review and further references) rely on an extended symmetry $\mathcal{G}$ broken to a subgroup $\mathcal{H}$. The KK gauge bosons $A_\mu^{\hat{a}}$ associated with the coset directions $\mathcal{G}/\mathcal{H}$ are all massive, but the $A_5^{\hat{a}}$ towers give rise to zero modes. The latter are 4D scalars and, by an appropriate choice of the symmetry breaking pattern $\mathcal{G} \to \mathcal{H}$, can have the correct quantum numbers to be identified as the Higgs. The higher-dimensional gauge symmetry leaves a remnant shift symmetry for the Higgs [24] that ensures that the Higgs potential is finite to all orders. This UV insensitivity guarantees that the Higgs potential gets corrections of the order of the IR scale $\mu_{\rm IR}$ and not the cutoff of the theory, thus alleviating (though not solving) the little hierarchy problem. In this paper we will show how our construction can be easily implemented in a fully realistic model of GHU in warped extra dimensions. We will consider the minimal composite Higgs model with fermions in the fundamental representation of $SO(5)$ (MCHM_5) of Ref. [25], but our construction could be applied to other variations such as the models considered in [26]. The starting bulk gauge group is $SO(5) \times U(1)_X$, broken to $SO(4) \times U(1)_X$ on the IR brane [the actual symmetry on the IR brane is assumed to be $O(4)$] and to the SM on the UV brane. The quark sector is embedded in fundamental representations of $SO(5)$ that decompose under $SO(4) \sim SU(2)_L \times SU(2)_R$ as a bidoublet plus a singlet, $\mathbf{5} = (2,2) \oplus (1,1)$. The relevant sector for EWSB is the third generation. See Appendix A for a summary of the field content of the model.

Let us now construct the simplest $\mathbf{Z}_2$ extension of the MCHM_5 model. Following our prescription, we enlarge the gauge group by doubling the $U(1)_X$ factor to $U(1)_{X_1} \times U(1)_{X_2}$ and identify the original gauge boson X with the even combination, $X_+ = \frac{1}{\sqrt{2}}(X_1 + X_2)$. The odd combination has $(+,-)$ boundary conditions as in Eq. (2.4). As emphasized in the previous section, only fermions with mass parameter $|c| < 1/2$ can be safely doubled, since otherwise they could easily give rise to charged/colored $\mathbf{Z}_2$-odd KK modes lighter than the $\mathbf{Z}_2$-odd KK gauge bosons. It is therefore natural to consider doubling the multiplets associated with the top quark, since accommodating the top mass requires $|c| < 1/2$ for the associated 5D fields. By looking at Eq. (A5), it is clear that the only field that can be doubled without introducing new unwanted zero modes is ξ_u. We will see that this is sufficient to obtain the correct DM relic density. In summary, our quark sector is identical to that of the MCHM_5 model, except that ξ_u is replaced by two copies ξ_{u_1} and ξ_{u_2}, with $U(1)_{X_1} \times U(1)_{X_2}$ charges $(2/3, 0)$ and $(0, 2/3)$, respectively, but otherwise identical in boundary conditions and bulk mass. The physical combinations are the $\mathbf{Z}_2$-even ξ_u^+ (which, for simplicity, we will call ξ_u in what follows) and the $\mathbf{Z}_2$-odd ξ_u^-. The other quark and lepton fields are assigned the same charge under both Abelian groups, $(\frac{1}{2}Q_X, \frac{1}{2}Q_X)$, where $Q_X = 2/3$ for ξ_{q_1}, $Q_X = -1/3$ for ξ_{q_2} and ξ_d, and analogous assignments for the lepton sector. Therefore, the spectrum in our model contains a set of fields that are even under the $\mathbf{Z}_2$ symmetry and corresponds exactly to the spectrum in the original MCHM_5 model, plus two 5D $\mathbf{Z}_2$-odd multiplets X_- and ξ_u^-. The $\mathbf{Z}_2$-odd gauge boson has a first KK mode, which we will simply call X_-, with a mass given by Eq. (2.5). The $\mathbf{Z}_2$-odd fermions have first KK modes with c_u-dependent masses that are, neglecting EWSB effects and provided $|c_u| < 1/2$, always larger than the one of X_-.[7] As we take $c_u \to 1/2$ the first KK mode of $(2,2)^{u_-}$ becomes degenerate with X_-, whereas in the $c_u \to -1/2$ limit it is $(1,1)^{u_-}$ that becomes degenerate with X_- (see Appendix A for the notation).

[6] In principle, it is also possible to introduce $\mathbf{Z}_2$-odd fermions with $(++)$ boundary conditions, getting rid of the zero modes by coupling them through mass terms to localized chiral fermions. In the limit that these masses become large, a description by effective b.c. as the one we are using is appropriate.

[7] Note that odd-fermion masses are independent of the localized mixing masses, and are therefore entirely determined by c_u, up to EWSB effects. After the mixing due to EWSB, these could become lower than m_{X_-} if $|c_u|$ is very close to $1/2$.

A. Electroweak symmetry breaking and precision constraints

The pattern of EWSB in the MCHM$_5$ model and its main constraints have been studied in [25–27]. A realistic pattern of EWSB can be obtained for $|c_{q_1}| \lesssim 0.4$ and $0.35 \lesssim |c_u| \lesssim 0.45$. Outside these two regions, it is difficult to obtain a reasonable value of the gauge boson, top and Higgs masses. Of particular interest is the dependence on c_u. For fixed values of the other parameters, smaller values of $|c_u|$ result in no EWSB, while larger values of $|c_u|$ give the wrong EWSB pattern. The qualitative features of this dependence can be easily understood in the limit that the localized mixing masses vanish. In this simplified case, the two chiralities of the top quark arise from ξ_{q_1}, and obtaining a top Yukawa coupling of order one fixes $c_{q_1} \approx 0.44$. The contribution to the Higgs potential due to the ξ_{q_1} KK tower destabilizes the origin, while the contributions from the gauge KK towers tend to align the vacuum along the EW symmetry-preserving direction. It turns out that the top tower contribution is so large that it would drive the vacuum expectation value (VEV) to its maximum value $s_h = 1$, where

$$s_h = \sin\left(\frac{\langle h\rangle}{f_h}\right), \qquad f_h = \frac{1}{g}\sqrt{\frac{2}{kL}}\mu_{\rm IR}. \tag{3.1}$$

Here f_h is the "Higgs decay constant" and g is the SM $SU(2)_L$ gauge coupling. The resulting EW symmetry breaking pattern is unacceptable since it leads to vanishing fermion masses, and highly nonlinear couplings of the Higgs to the gauge bosons that are ruled out by EW precision measurements. However, fermions with "twisted" boundary conditions, such as ξ_u, give a contribution to the Higgs potential that tends to align the vacuum along the EW symmetry-preserving direction. This contribution is controlled only by c_u in the above simplified limit, and turns off when $|c_u| \gtrsim 1/2$. If $|c_u| \ll 1/2$, then this EW restoring contribution overwhelms the contribution due to ξ_{q_1} and results in $s_h = 0$. The upshot is that the desired EWSB VEV $0 < s_h < 1$ is obtained for $|c_u| \sim 1/2$, but not necessarily too close to $1/2$. This also illustrates the crucial role that ξ_u plays for EWSB. When the mixing masses are turned on the details are more complicated, but the qualitative features remain the same. See Appendix B for details on the computation of the Higgs potential.

On the other hand, EW precision data typically prefer values of $|c_u|$ close to $1/2$. This is due to a sizable and negative one-loop contribution to the Peskin-Takeuchi [28] T parameter in most regions of parameter space [29], together with a non-negligible tree-level *positive* contribution to the S parameter. The tree-level contribution to S, when the light fermions are localized close to the UV brane, is given by [6]

$$S_{\rm tree} \approx \frac{6\pi s_h^2}{g^2 kL} \approx \frac{3\pi v^2}{\mu_{\rm IR}^2}, \tag{3.2}$$

where the second equality holds whenever $v = \langle h\rangle \sim 174$ GeV $\ll f_h$. The negative contribution to the T parameter arises at one-loop order from the lightest charge-$2/3$ members of the $SU(2)_L \times SU(2)_R$ bidoublets, and is dominant away from the $|c_u| \sim 1/2$ region. Additionally, the pseudo-Goldstone nature of the Higgs leads to a further negative (positive) contribution to the T (S) parameter, due to the anomalous gauge couplings of the Higgs [30]. This can be described by an effective Higgs mass [31]

$$m_{h,\rm eff} = m_h\left(\frac{\Lambda}{m_h}\right)^{s_h^2}, \tag{3.3}$$

where Λ is an effective cutoff scale of the order of the mass of the first SM gauge KK resonances $m_{\rm KK}$, so that the corresponding shifts in S and T are

$$\Delta S_h = \frac{1}{12\pi}\ln\left(\frac{m_{h,\rm eff}^2}{m_{h_{\rm ref}}^2}\right), \qquad \Delta T_h = -\frac{3}{16\pi c_W^2}\ln\left(\frac{m_{h,\rm eff}^2}{m_{h_{\rm ref}}^2}\right).$$

Here $m_{h_{\rm ref}}$ is the reference Higgs mass used in the S-T fit to the EW data, and c_W is the cosine of the Weinberg angle.

The S-T analysis reveals that in the $\mathbf{Z}_2$ extended MCHM$_5$ model, the regions with $|c_u| \sim 1/2$ are preferred (see Fig. 1). For $c_u \sim -1/2$, the reason can be traced back to the fact that the first KK excitation of the $SO(4)$ *singlet* in ξ_u, that mixes with the top quark, becomes light and gives a positive contribution to the T parameter that compensates the negative contributions coming from the lightest bidoublet states and effective heavy Higgs, Eq. (3.3). As a result, one finds a sizable region in parameter space compatible with EWSB, where the EW precision measurements are relaxed. For $c_u \sim 1/2$, it is again possible to satisfy the EW constraints, although the reason is somewhat more involved than for $c_u \sim -1/2$. As emphasized in [29], the charge-$2/3$ members of the bidoublets give rise to both positive (from the $T_L^3 = +1/2$, $T_R^3 = -1/2$ states) and negative (from the $T_L^3 = -1/2$, $T_R^3 = +1/2$ states) contributions to T. In the custodially symmetric limit these two contributions would cancel exactly, but in most regions the fact that the $T_L^3 = -1/2$ state is lighter than the $T_L^3 = +1/2$ one typically results in a net negative contribution to T (the signs are simply determined by the quantum numbers). However, when $c_u \sim 1/2$, the lightest bidoublets arise mostly from ξ_u (and therefore have a nearly flat wave function component, that vanishes on the IR brane), and lead to a contribution to T via mass mixing with the bidoublet in ξ_{q_1}. It is then possible to suppress the coupling to the Higgs of the lighter $T_L^3 = -1/2$ state by ensuring that it lives mostly in the component with the nearly flat wave function, while the heavier $T_L^3 = +1/2$ state has a larger component in the bidoublet of the ξ_{q_1} multiplet, that is localized near the IR brane. In this way, the positive

contribution due to the $T_L^3 = +1/2$ state can dominate, and explains how the $c_u \sim 1/2$ region can be compatible with the EW precision data with a relatively low scale.[8]

In addition to the oblique corrections parametrized by S and T, nonoblique corrections associated with the third generation can also be relevant. These can be separated into flavor-preserving versus flavor-violating effects. A complete treatment of the latter would require the specification of the flavor structure of the model, which is beyond the scope of this paper. Most notable among the flavor-preserving effects are the corrections to the $Z\bar{b}_L b_L$ vertex, which has been measured at the few per mille level. Here we notice that the present model enjoys the custodial protection pointed out in [4], which reduces the tree-level corrections to this vertex to a level well below the experimental precision. However, as first pointed out in [26,29] (see also [31]) the one-loop contributions to this vertex can be significant and correlated with the one-loop contribution to the T parameter discussed above. Hence, we also include these effects in the fit to the EW precision observables, although, for the reasons explained above, we do not include flavor-violating effects.[9] In this analysis we have performed a fit to the Z-pole observables and the W mass [33], and include the effects of four-fermion interactions that enter through the Fermi constant (these effects are subdominant). The upshot is that there is a bound of about $\mu_{\rm IR} \sim 1.3$ TeV in the $c_u > 0$ region, while the $c_u < 0$ region is somewhat more constrained, with a lower bound $\mu_{\rm IR} \sim 1.7$ TeV.

Notice that although the $\mathbf{Z}_2$-odd fermions do not contribute to T (since the b.c. for ξ_u^- respect the custodial symmetry exactly and there is no mixing with custodial violating sectors of the theory due to the exact $\mathbf{Z}_2$ symmetry), they affect the minimization of the Higgs potential in an analogous way to ξ_u, discussed at the beginning of this section. In particular, the existence of these additional fields satisfying twisted b.c., and whose effects on the Higgs potential are controlled also by c_u, means that the minimization of the potential favors values of $|c_u|$ that are closer to $1/2$ than if the $\mathbf{Z}_2$-odd fermions were absent. This is a welcome feature, since it goes in the direction preferred by the EW precision data, as discussed above. Furthermore, the opening of a well-defined region with $c_u \sim 1/2$, where the (t_L, b_L) doublet is more fundamental [see $f_L^+(z)$ in Eq. (C2)] is also welcome since it might be argued, based on flavor considerations, that such a situation is more natural.

Thus, we find that the regions that lead to a correct EWSB pattern and good agreement with the EW precision data largely overlap in the $\mathbf{Z}_2$ extension of the MCHM$_5$ model. We postpone a discussion of the details associated with Fig. 1 to the next section, after we have discussed the computation of the DM relic density in this scenario. For the moment, let us mention that we predict relatively light vectorlike quarks (from both ξ_u and ξ_u^-) with masses close to $m_{X_-} \sim \sqrt{2/kL}\,\mu_{\rm IR}$, a very distinctive signature of these models. It should also be emphasized that our model has the same number of parameters as the MCHM$_5$ without DM.

B. Calculation of the relic abundance

As was discussed in the previous section, a realistic pattern of EWSB requires $|c_u| \lesssim 1/2$. Thus, we have two separate regions that, *a priori*, could give rise to phenomenologically relevant scenarios. This can have important consequences for the computation of the DM relic abundance since, as remarked above, some of the $\mathbf{Z}_2$-odd fermions become degenerate with the DM candidate when $|c_u| = 1/2$. In the case $c_u \sim -1/2$, it is the first KK mode of the $SO(4)$ singlet component of ξ_u^- that becomes close in mass to X_- (the LOP), while the KK modes of the bidoublet are at least a factor of 10 or so heavier. In the other relevant region of parameter space $c_u \sim 1/2$ (composite t_R), the situation is inverted, with the first KK modes of the members of the bidoublet of ξ_u^- becoming light, while the singlet is considerably heavier. These $\mathbf{Z}_2$-odd quarks couple to X_- and SM fermions (top or bottom), and we will refer to the lightest of them as the NLOP (next-to-lightest odd particle). Depending on the degree of degeneracy, coannihilation effects can be relevant to obtain the DM relic abundance. Note that for $c_u > 0$, there are several states whose masses are split only by EWSB effects, and all of them can affect the final DM relic density.

In order to get an order of magnitude estimate, we start by assuming that coannihilation processes can be neglected (a reasonable approximation whenever the $\mathbf{Z}_2$-odd quarks are heavier than X_- by a factor of $\gtrsim 15\%$). In this case, the only relevant process for the calculation of the DM relic abundance is the annihilation of X_- pairs into SM quarks, via NLOP exchange. Up to EWSB effects, which can be shown to give negligible corrections, the relevant 5D interactions are

$$\overline{(1,1)}^{u}_{R} \not{X}_- (1,1)^{u_-}_{R} + \text{H.c.}, \tag{3.4}$$

for $c_u \sim -1/2$, and

$$\overline{(2,2)}^{u}_{L} \not{X}_- (2,2)^{u_-}_{L} + \text{H.c.}, \tag{3.5}$$

[8]This important positive contribution is not present in the minimal models studied in Ref. [31] (it is, however, in models with a custodial protection of the $Z\bar{b}_L b_L$ coupling as the one we are considering).

[9]Nevertheless, we have checked that a subset of the flavor-violating corrections, that are closely connected to parameters entering in the flavor-preserving effects [31], do not significantly alter the bounds. Specifically, these include certain loop-level contributions to the $Z\bar{b}s$ vertex that are bound by $B \to X_s l^+ l^-$ decays (these are likely to be more important in the $c_u < 0$ region), as well as tree-level contributions to the $W\bar{t}_R b_R$ vertex, that can be bound from the $B \to X_s \gamma$ branching ratio [32] (these affect mostly the $c_u > 0$ region).

for $c_u \sim 1/2$. Here $(1,1)^u_R$ and $(2,2)^u_L$ contain, respectively, the right-handed (RH) top and the left-handed (LH) top and bottom zero modes. We denote by $\tilde{g}_L$ and $\tilde{g}_R$ the 4D couplings between the LOP, NLOP and top/bottom quarks, arising from Eqs. (3.4) and (3.5), respectively. These are the crucial couplings entering in the self-annihilation cross section of X_-. In the absence of UV brane kinetic terms, both $\tilde{g}_L$ and $\tilde{g}_R$ are bound from above as follows:

$$|\tilde{g}_{L,R}| \lesssim \frac{2}{3} g_X = \frac{2}{3} \frac{g g'}{\sqrt{g^2 - g'^2}} \approx 0.28, \tag{3.6}$$

where g_X is the $U(1)_X$ gauge coupling that we have also written in terms of the SM $SU(2)_L \times U(1)_Y$ gauge couplings. We refer the reader to Appendix C for a detailed derivation of the couplings $\tilde{g}_L$ and $\tilde{g}_R$. They are typically of the same size, so that the main difference between the above two regions is the presence of one decay channel (into t_R) for $c_u < 0$, and two (into t_L and b_L) in the $c_u > 0$ case. For this reason, it will be useful in the following to define the parameter η, such that $\eta = 1$ for $c_u < 0$ and $\eta = 2$ for $c_u > 0$, and write the coupling simply as $\tilde{g}$, with the understanding that $\tilde{g} = \tilde{g}_R$ for $c_u < 0$ and $\tilde{g} = \tilde{g}_L$ for $c_u > 0$.

The computation of the DM relic abundance is standard (see e.g. [34]). In the freeze-out approximation, it can be written in terms of the coefficients of the nonrelativistic expansion of the annihilation cross section, $\sigma(X_- X_- \to SM)$,

$$v\sigma = a + v^2 b + \cdots, \tag{3.7}$$

as

$$\Omega h^2 \approx \frac{1.04 \times 10^9}{M_P} \frac{x_F}{\sqrt{g_*}} \frac{1}{a + 3b/x_F}, \tag{3.8}$$

where $M_P \approx 1.22 \times 10^{19}$ GeV is the Planck mass, $x_F = m_{X_-}/T_F$, with T_F the freeze-out temperature (in our case, with $\lesssim$ TeV weakly interacting particles, $x_F \sim 24 - 26$), g_* is the effective number of relativistic degrees of freedom at freeze-out ($g_* = 86.25$ for 100 GeV $\lesssim m_{X_-} \lesssim$ TeV) and a and b are measured in GeV^{-2}. Neglecting EWSB effects, the annihilation cross section depends on $\tilde{g}$, m_{X_-} and the mass of the lightest modes in ξ^-_u, which we call m_ψ. It turns out that the factor b gives a negligible effect. Denoting

$$\Delta \equiv \frac{m_\psi - m_{X_-}}{m_{X_-}}, \tag{3.9}$$

we obtain

$$a = \frac{2\eta \tilde{g}^4}{3\pi} \frac{1}{(1 + (1+\Delta)^2)^2} m^{-2}_{X_-}, \tag{3.10}$$

and

$$\Omega h^2 \approx \frac{0.15}{\eta} \left(\frac{m_{X_-}}{400\ \text{GeV}}\right)^2 \left(\frac{0.28}{\tilde{g}}\right)^4 \left(\frac{1 + (1+\Delta)^2}{1 + (1+0.15)^2}\right)^2. \tag{3.11}$$

This result is actually very accurate. Using the full expression for the annihilation cross section and the freeze-out temperature, we obtain, again assuming that the difference in mass between X_- and the $\mathbf{Z}_2$-odd quarks is $\gtrsim 15\%$,

$$\Omega h^2 \gtrsim \begin{cases} 0.16\ (0.6), & c_u < 0, \\ 0.08\ (0.28), & c_u > 0, \end{cases} \tag{3.12}$$

where we assumed $m_{X_-} \gtrsim 400$ GeV, and the numbers are for $\tilde{g} = 0.28$ (maximal coupling) and, in parenthesis, for $\tilde{g} = 0.2$. We therefore see that the observed relic abundance [35]

$$\Omega_{\text{DM}} h^2 = 0.1143 \pm 0.0034 \tag{3.13}$$

can be accounted for with just X_- annihilation for $c_u > 0$, provided $\tilde{g}$ is large enough. For $c_u < 0$, the observed DM energy density seems more difficult to accommodate in the simplest scenario where only X_- annihilations are relevant.[10] However, as explained above, EWSB and the EW precision measurements independently point to a region in parameter space with one or more vectorlike quarks that are nearly degenerate with the LOP, and a proper determination of the relic abundance should take coannihilation effects into account [36]. This is welcome because, due to the colored nature of the new particles, coannihilations tend to increase the cross section and therefore decrease the relic abundance to values compatible with observation for smaller couplings and/or larger m_{X_-}.

The relevant processes that enter the relic abundance computation are $X_- X_- \to t\bar{t}(b\bar{b})$, $X_- \psi_- \to gt(gb)$, $X_- \bar{\psi}_- \to g\bar{t}(g\bar{b})$, $\psi_- \bar{\psi}_- \to q\bar{q}$ and $\psi_- \bar{\psi}_- \to gg$, where ψ_- stands for any of the $\mathbf{Z}_2$-odd fermions that are nearly degenerate with X_-, g is the SM gluon and $q\bar{q}$ are SM quark-antiquark pairs. The relevant effective annihilation cross section reads

$$\begin{aligned} \sigma_{\text{eff}} = \frac{1}{g^2_{\text{eff}}} \Big[& 9\sigma_{X_- X_- \to t\bar{t}} + 9(\eta - 1)\sigma_{X_- X_- \to b\bar{b}} \\ & + 72 e^{-x\Delta}(1+\Delta)^{3/2} \sigma_{X_- \psi_- \to gt} \\ & + 72(\eta - 1) e^{-x\Delta}(1+\Delta)^{3/2} \sigma_{X_- \psi_- \to gb} \\ & + 72\eta^2 e^{-2x\Delta}(1+\Delta)^3 \left(\sum_q \sigma_{\psi_- \bar{\psi}_- \to q\bar{q}} + \sigma_{\psi_- \bar{\psi}_- \to gg} \right) \Big], \\ g_{\text{eff}} = 3 + 12\eta^2 e^{-x\Delta}(1+\Delta)^{3/2}, & \end{aligned} \tag{3.14}$$

where $x = m_{X_-}/T$, and Δ was defined in Eq. (3.9). In

[10] We note that the presence of kinetic mixing between the two $U(1)$ factors, or UV brane localized kinetic terms for them, can change the coupling relevant for annihilation of LOPs, leading to a realistic DM relic abundance. We assume that such terms are small, so that no relevant additional parameters are introduced.

Eq. (3.14), the factor η introduced before takes into account that in the $c_u < 0$ region there is a single $\mathbf{Z}_2$-odd fermion with $m_{\psi_-} \approx m_{X_-}$, whereas for $c_u > 0$ there are four fermions with $m_{\psi_-} \approx m_{X_-}$. When $c_u > 0$, Eq. (3.14) is valid in the limit in which we neglect the mass splitting between the fermions of the bidoublet (which arises only from EWSB effects) and it is understood that the cross sections with final state top (bottom) quarks involve the $Q = 2/3$ ($Q = -1/3$) heavy vectorlike fermions.

We performed exhaustive scans, computing the pattern of EWSB, the fit to EW precision data, the DM relic abundance and the spectrum of light quarks. In order to more easily automatize the scan over large regions of parameter space while taking into account coannihilations, we found it useful to implement the relevant features of our model in MICROMEGAS [37]. This also allows us to easily take into account the mass splittings arising from EWSB among the lightest bidoublet states that are relevant in the $c_u \sim 1/2$ region, as well as nonzero final state masses (for the typical scales of $m_{X_-} \sim 400$ GeV, the top mass can be important). We have checked independently that we reproduce the MICROMEGAS results for the relic density to within 10% using Eq. (3.14), in the limit that EWSB mass splitting effects are neglected, and in the freeze-out approximation.

We present the results separately for the two phenomenologically interesting regions discussed previously, namely, $c_u \sim -1/2$ and $c_u \sim 1/2$. We scanned over the following region in parameter space: $c_{q_1} \in [0, 0.4]$, $c_{q_2} \in [0.4, 0.5]$, $|c_u| \in [0.45, 0.5]$, $c_d \in [-0.52, -0.45]$, $|m_u| \leq 1$, $|M_u| \leq 1$, $|m_d| \leq 0.5$, $|M_d| \leq 0.5$, with $kL \approx 34$ in order to explain the Planck-weak scale hierarchy. We show the results of the scan as a projection onto the c_u-c_{q_1} plane in Fig. 1, where the red triangles correspond to the data consistent with the three-year Wilkinson microwave anisotropy probe (WMAP) results, Eq. (3.13), at the 2σ level.

We also highlight in the plot the data that have $145\ \text{GeV} < m_t(\mu \sim \mu_{\text{IR}}) < 155\ \text{GeV}$ (green dots). As we will discuss further in Sec. III D, the top mass plays a rather important role in leading to a vacuum with appropriate characteristics in these scenarios. In the background of the figure we exhibit in gray tones information about the degree of EWSB as measured by s_h [see Eq. (3.1)]. In order to make the projection onto the c_u-c_{q_1} plane we show the average of s_h, computed over the rest of the parameters in the scan. In particular, in the darker area marked as $s_h = 0$, all points in the scan lead to an EW symmetry-preserving vacuum. For $c_u < 0$ ($c_u > 0$), the degree of EWSB, in the above sense, increases as one moves towards the bottom left (right) corner of the figure (lighter grays correspond to larger average s_h). We therefore see that in most of the region with nontrivial EWSB the correct top mass can be reproduced. Even more interestingly, the area selected by the observed DM abundance falls in precisely the same region. This is related to the fact that coannhilations play a relevant role in lowering the DM abundance to the observed level compared to the estimates Eq. (3.12) and, as explained before, this happens naturally in the above region (we did not compute the DM relic abundance for points with $s_h = 0$).

Finally, we also show in the figure information about the fit to the EW precision data. As explained in Sec. III A, we include in our fit the universal corrections described by the S and T parameters and the correction to the $Z\bar{b}_L b_L$ vertex (both tree- and one-loop contributions), performing a $\Delta\chi^2$ cut at 99% C.L. with 3 d.o.f. Since this analysis is computationally intensive, we performed the EW test only for points that satisfy $149.5\ \text{GeV} < m_t(\mu \sim \mu_{\text{IR}}) < 150.5\ \text{GeV}$ (without imposing the WMAP constraint), and for $145\ \text{GeV} < m_t(\mu \sim \mu_{\text{IR}}) < 155\ \text{GeV}$ when the WMAP constraint, Eq. (3.13), is imposed. The selection of the very narrow range in the first case is done only in

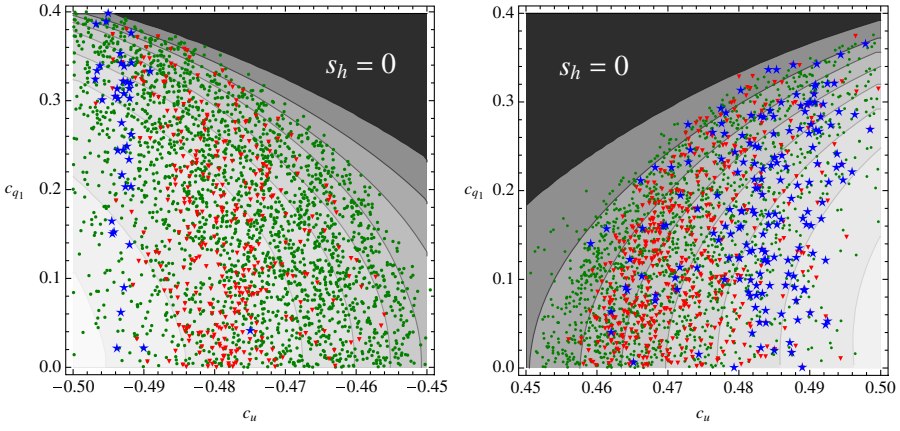

FIG. 1 (color online). Projection onto the c_u-c_{q_1} plane for the two phenomenologically viable regions. The darker areas marked $s_h = 0$ correspond to no EWSB. We plot s_h averaged over the rest of the parameters, which increases as the gray bands become lighter (see text). The green dots satisfy $145\ \text{GeV} < m_t(\mu \sim \mu_{\text{IR}}) < 155\ \text{GeV}$. The red triangles mark the points consistent with the WMAP constraint, Eq. (3.13), at the 2σ level. The blue stars correspond to a sample of points that are consistent with EW precision data at the 99% C.L., and the Higgs LEP bound.

order to reduce the number of points to be analyzed, but it should nevertheless give a clear picture of the situation. We also require that the Higgs mass be above the LEP bound $m_h > 114.4$ GeV. Requiring that the DM relic abundance be in the range (3.13), we find that in the $c_u > 0$ ($c_u < 0$) region about 25% (15%) of the points pass the EW precision test at the 99% C.L. Thus, we conclude that in the present model, the correct EWSB pattern, consistency with the EW precision measurements, and the correct DM abundance all occur in a common region of parameter space. This leads to a rather compelling picture with a light neutral spin-1 DM candidate, and one or more fermionic resonances that are nearly degenerate with the DM particle. We will briefly discuss their collider phenomenology in Sec. V.

Two important physical observables that are relatively well predicted in our scenario are the Higgs mass and the mass of the DM candidate. We show in Fig. 2 the distribution of points with a realistic EWSB pattern (including the top mass) that reproduce the observed DM relic density, in the $m_{X_-} - m_h$ plane. We also highlight the subset of points that are consistent with the EW precision constraints at the 99% C.L. We see that the LEP bound on the Higgs mass is easily evaded in our scenario. Also, the Higgs boson is expected to be lighter than about 170 GeV. The mass of the DM particle is expected to be somewhat above 300 (400) GeV for $c_u > 0$ ($c_u < 0$). As was mentioned above, there is a number of vectorlike quarks nearly degenerate with the LOP. We also indicate in Fig. 2 the approximate direct Tevatron bound on such particles. Although the direct bound already excludes a significant region in parameter space, the EW precision analysis still puts stronger constraints on the masses of these particles. It is also useful to remember that, for $kL \approx 34$, we have $m_{X_-} \approx 0.24\mu_{\rm IR}$, which shows that $\mu_{\rm IR} \gtrsim 1.3$ TeV ($\mu_{\rm IR} \gtrsim 1.7$ TeV) for $c_u > 0$ ($c_u < 0$). Recall also that, in the absence of brane kinetic terms, other spin-1 resonances have a mass $m_{\rm KK} \approx 2.5\mu_{\rm IR} \gtrsim 3.1$ TeV ($m_{\rm KK} \gtrsim 4.2$ TeV) for $c_u > 0$ ($c_u < 0$).

C. Nonperturbative corrections

There are various physical processes that might possibly invalidate the standard computation of the relic density based on perturbative averaged cross sections, namely, the formation of bound states and higher order corrections relevant for nonrelativistic particles. Such effects do not directly affect the physics of our DM candidate X_-, but they can affect the physics of the NLOP, which is a charged and colored fermion. Since coannihilations have to be taken into account in our setup, it is important to estimate the above effects. We will not perform a detailed quantitative study of bound state formation at finite temperature since, as we will argue below based on qualitative estimates, such effects can most likely be neglected. On the other hand, certain higher order corrections, which take into account the long-range Coulomb-like forces of QCD in the deconfinement phase, are potentially relevant. We find, however, that their eventual contribution to the perturbative cross sections is very small. Since strong interactions play the major role, we will neglect in this subsection the effects due to electroweak interactions.

Let us first consider the issues associated with the formation of bound states. The potential problem is very simple. If metastable, $\mathbf{Z}_2$-even, bound states of two NLOP particles can form, their decay through the self-annihilation of its constituents would lead to an effective depletion of $\mathbf{Z}_2$-odd particles, consequently reducing the DM relic density. Bound state effects of DM colored particles (gluinos) have been previously considered in [38], in connection with relic density computations, and were shown to have the potential to reduce the final DM density by orders of magnitude compared to the perturba-

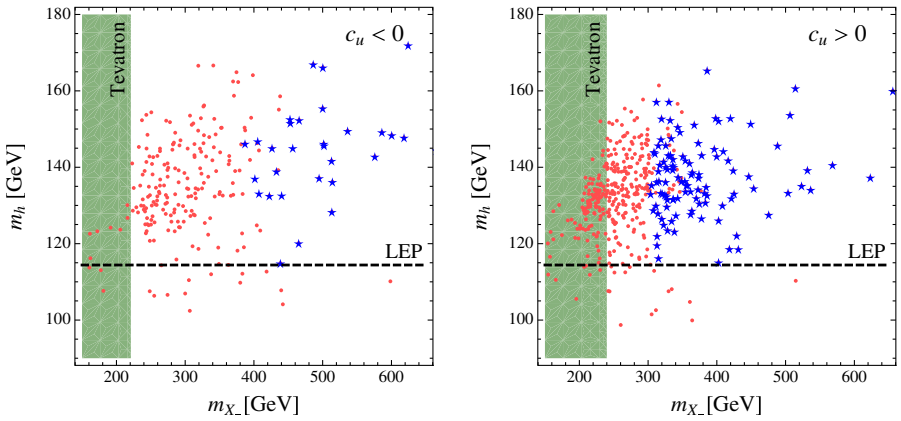

FIG. 2 (color online). Masses of the DM candidate X_- and the Higgs for points (red dots) that reproduce the top mass and the WMAP constraint, Eq. (3.13), for the $c_u < 0$ region (left panel) and $c_u > 0$ region (right panel). The blue stars correspond to the subset of points that also obey the EW precision constraints at the 99% C.L., and the LEP bound on the Higgs mass, which is also indicated by the dashed horizontal line. The light bands indicate the approximate bounds from the Tevatron on the colored vectorlike quarks, that have mass close to m_{X_-}, taking into account the different multiplicities for positive and negative c_u.

tive estimate. The crucial difference here is that the NLOPs are unstable, and as we argue below they decay into LOPs well before they have time to form bound states. The NLOP can decay via intergenerational mixing into the LOP and a light quark (decays into tops are forbidden by phase space in the quasidegenerate region of interest to us). To lowest order in Δ, as defined in Eq. (3.9), the NLOP lifetime is

$$\tau_\psi \approx \frac{8\pi}{3\lambda^2}\frac{m_\psi^{-1}}{\Delta^2} \simeq \frac{2\times 10^{-23}}{\lambda^2}\ \text{sec}, \tag{3.15}$$

where $\lambda^2 = \sum_{q=c,u}(g_{qL}^2 + g_{qR}^2)$ is the (model-dependent) coupling of the NLOP to the up and charm quarks, and the number quoted is obtained by taking a rather degenerate case, $m_{X_-} = 350$ GeV and $m_\psi = 360$ GeV.

We estimate next the time scale when the (NLOP-NLOP) bound states would become metastable. A reasonable criterion is to assume that these bound states are metastable against thermal fluctuations when the temperature drops below their binding energy E_{bind}. Since the bound state system is nonrelativistic, and in fact the scales are such that the QCD interactions are in the perturbative regime, we can estimate E_{bind} in analogy to positronium.[11] The color Coulomb force between two quarks in a color singlet state are obtained from the usual Coulomb potential by the replacement $\alpha \to (4/3)\alpha_s(p)$. Here $\alpha_s(p)$ is evaluated at the typical momentum scale of the virtual gluons responsible for the Coulomb-like interactions, which is $p \sim m_\psi\alpha_s(p)/2$. For $m_\psi \simeq 400$ GeV—the typical scale in our scenario—one gets $p \simeq 30$ GeV and $\alpha_s(p) \simeq 0.14$. The binding energy is then given by

$$E_{\text{bind}} \simeq \tfrac{1}{4}(\tfrac{4}{3})^2\alpha_s(p)^2 m_\psi \sim 10^{-2} m_\psi. \tag{3.16}$$

Thus, the (NLOP-NLOP) bound states become metastable *after* freeze-out, which occurs when $T \sim m_\psi/25$. In this radiation-dominated era, these two events happen at times $t \sim 10^{-7}$ sec and $t \sim 4\times 10^{-9}$ sec in the evolution of the Universe, respectively. It is therefore clear from Eq. (3.15) that for any reasonable value of the model-dependent coupling λ, the NLOPs decay into LOPs immediately after freeze-out, and well before bound states can become metastable.

The second effect we consider is due to the long-range Coulomb interactions that, for sufficiently nonrelativistic particles, can distort their wave functions from the plane wave shape and alter the standard quantum field theory perturbative computation of scattering processes. Such an effect is well-known and was first analyzed by Sommerfeld in the QED context [39]. It has recently been considered, in connection with relic density computations, in [40] for electroweak interactions and in [38] for strong interactions. For QED at zero temperature, the "Sommerfeld" effect can be encoded in an effective parameter S which reads, for absolutely stable particles,[12]

$$S = -\frac{\pm x}{1 - e^{\pm x}}, \tag{3.17}$$

with $x = \pi\alpha/v$, v the velocity of the colliding particles in the center of mass frame, and $\pm$ refer to repulsive or attractive Coulomb forces, respectively. Given a cross section σ computed in the standard perturbative fashion between charged nonrelativistic initial states, the replacement $\sigma \to S\sigma$ is an effective way to take into account the Coulomb forces, assuming relativistic final states. In a relativistic approach, the Sommerfeld factor S is obtained by resumming an infinite class of Feynman diagrams ("ladder" diagrams). From Eq. (3.17), it is clear that S is non-negligible only for sufficiently nonrelativistic particles. Cold DM candidates are by definition nonrelativistic at freeze-out and the Sommerfeld effect can play a role, as emphasized in [38,40]. For strong interactions in a perturbative regime, an analysis along the lines of QED can be made. By neglecting screening effects due to temperature (which is a good approximation at T_f; see also footnote [11]), Eq. (3.17) still holds, with the replacement $\alpha \to C_r\alpha_s(p)$ in x, where C_r is a color factor that depends on the $SU(3)$ representation of the particles involved, and $p \simeq mv$ is the typical momentum of the virtual gluons responsible for the Sommerfeld effect in a relativistic treatment [38]. For a $\psi - \bar{\psi}$ pair in the initial state, one can have either a singlet or an octet $SU(3)$ configuration, with color factors $C_{\mathbf{1}} = 4/3$ and $C_{\mathbf{8}} = -1/6$, respectively, At freeze-out, $v \simeq \sqrt{2T_f/m_\psi} \simeq 0.25$ and we get, for $m_\psi \simeq 400$ GeV, $S_{\mathbf{1}} \simeq 2.3$ and $S_{\mathbf{8}} \simeq 0.9$. Thus, the Sommerfeld effect, especially in the singlet channel, is non-negligible. We have quantified the impact of the Sommerfeld effect on the computation of Ω by replacing the averaged tree-level cross sections as follows:

$$\sigma_{\psi\bar{\psi}\to\text{gluons}} \to \tfrac{1}{9}[S_{\mathbf{1}}\sigma_{(\psi\bar{\psi})_{\mathbf{1}}\to\text{gluons}} + 8S_{\mathbf{8}}\sigma_{(\psi\bar{\psi})_{\mathbf{8}}\to\text{gluons}}],$$
$$\sigma_{\psi\bar{\psi}\to q\bar{q}} \to \tfrac{1}{9}[S_{\mathbf{1}}\sigma_{(\psi\bar{\psi})_{\mathbf{1}}\to q\bar{q}} + 8S_{\mathbf{8}}\sigma_{(\psi\bar{\psi})_{\mathbf{8}}\to q\bar{q}}].$$

As it turns out, the enhancement of the cross sections in the

[11] Strictly speaking, at finite temperature there is a screening effect on charged particles, leading to an effective Debye mass for the gluon, $m_g \simeq \sqrt{2}g_s(T)T$. It is easy to check, however, that for $T/m_\psi \simeq 10^{-2}$ [see Eq. (3.16)], the thermal screening can be neglected.

[12] For unstable particles, one has to check whether the Sommerfeld effect has time to take place, by comparing the typical time scale of Coulomb interactions $t_{\text{Coulomb}} \sim 1/(Mv^2)$ with the decay time τ of the particle [41]. If $\tau \ll t_{\text{Coulomb}}$, the Sommerfeld effect has no time to take place. In our case, $\tau_{\text{NLOP}} \gg t_{\text{Coulomb}}$ and thus we can effectively treat the initial NLOP particles as absolutely stable.

attractive singlet channel is largely compensated by the repulsive octet channel, so that the effect on the final Ω is always very small (at most a few percent).

D. Fine-tuning

We established above that a rather well-defined region with $|c_u| \sim 1/2$ is simultaneously selected by the minimization of the Higgs potential, the EW constraints and the observed DM relic density. We should also recall that the pseudo-Goldstone nature of the Higgs allows for its mass to be parametrically lower than the scale of the KK resonances $\mu_{\rm IR}$, potentially alleviating the little hierarchy problem present in other RS constructions (of course, the large Planck-weak scale hierarchy is explained by the RS mechanism). It is therefore natural to ask how fine-tuned these scenarios really are. We quantify the fine-tuning at a given point in parameter space by considering the sensitivity to the microscopic parameters of the theory as measured by the logarithmic derivative [42]

$$\text{sensitivity} = \max\left\{\left|\frac{\partial \log\langle h\rangle}{\partial \log \lambda_i}\right|\right\}, \qquad (3.18)$$

where $\lambda_i = c_{q_1},\ c_{q_2},\ c_u,\ c_d,\ m_u,\ M_u,\ m_d,\ M_d$ are the fundamental parameters of the model. We find that the apparent fine-tuning is dominated by the sensitivity to c_u, as expected from our previous discussions. We show in the left panel of Fig. 3 the sensitivity parameter for the random scans described in Sec. III B, as a function of s_h. These show that throughout the region of parameter space that leads to phenomenologically viable EWSB breaking minima, the apparent fine-tuning is worse than a percent. Without tractable analytic expressions it is hard to identify precisely the nature of such sensitivity, and it is conceivable that the exponential nature of the warp factor gives rise to a generic sensitivity. In a 4D dual language, it would probably be related to the usual generic sensitivity which affects theories with a dynamical generation of scales, such as QCD or technicolor theories [43]. It is then possible that the fine-tuning estimate as given by Eq. (3.18) is too conservative and a more refined analysis is necessary. It would be interesting to investigate in more detail this issue.

However, we notice here that the sensitivity to the microscopic parameters seems to be almost exclusively related to the requirement of obtaining a large enough top Yukawa coupling. In order to illustrate the point, we compute again the logarithmic derivatives in the (c_u, M_u) plane, along directions with constant top mass. The result is shown in the right panel of Fig. 3. Although we have not explored the logarithmic derivatives at constant top mass in the whole parameter space and thus cannot exclude the existence of other directions where the sensitivity is higher, Fig. 3 shows that part of the fine-tuning in the model is associated with reproducing the observed top mass. Similar results also hold in the original MCHM$_5$ model without DM. We therefore conclude that the present model necessitates some degree of fine-tuning to reproduce the observed top mass, but once this measurement has been done, the physical properties of the resulting vacuum are fairly robust against variations in the microscopic parameters of the theory (observables other than $\langle h\rangle$ also exhibit this property). Notice that this is a single measurement associated with the zero-mode sector, and therefore there is a sense in which there is little sensitivity to the details of the new physics beyond the standard model. This also underscores the role that the heavy top plays in driving EWSB.

The above situation should be contrasted with SUSY scenarios that also present, generically, a sensitivity of order a percent to various fundamental parameters. In the

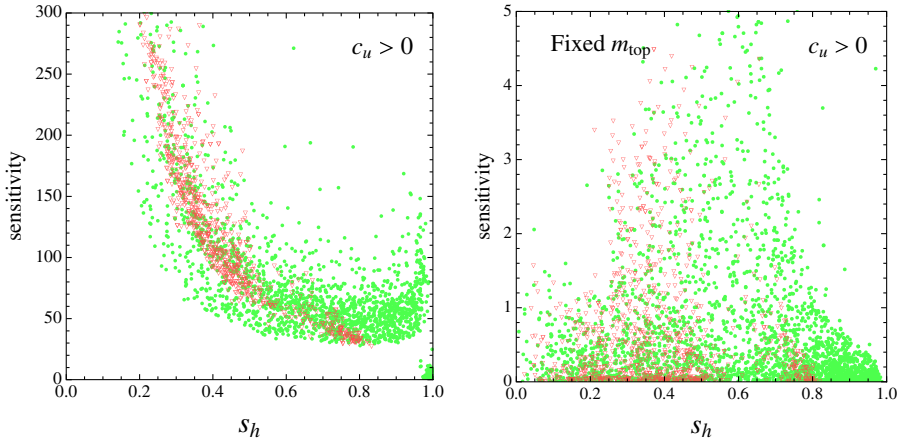

FIG. 3 (color online). Left panel: Logarithmic sensitivity as a function of s_h. Right panel: Logarithmic sensitivity with the requirement that the top mass be kept fixed (see text). The green dots correspond to a random scan over parameter space with $c_u > 0$. The subset that satisfies $140\ \text{GeV} < m_t(\mu \sim \mu_{\rm IR}) < 160\ \text{GeV}$ is indicated by red triangles. The results for the $c_u < 0$ region are similar.

SUSY case, reproducing a large top mass is no more difficult than in the SM (it is enough to choose the top Yukawa coupling, one of the "fundamental" parameters of these theories, to be of order one). However, there is a well-known intrinsic fine-tuning associated with a cancellation between the μ term and the soft SUSY breaking parameters in the Higgs sector. The latter depend quadratically on the stop soft SUSY breaking masses, which in turn need to be taken somewhat heavy (at least in the simplest SUSY extensions of the standard model) in order to get a large enough Higgs quartic coupling that allows satisfying the LEP bound on the Higgs mass. If, in addition, one takes into account the RG running from a high scale, and quantifies the fine-tuning by the sensitivity to the *high-energy* parameters of the theory, the situation worsens. In warped scenarios, the RS mechanism eliminates any possible fine-tuning due to running from a high scale. The dynamical generation of the weak scale in gauge-Higgs unification scenarios allows for a further natural separation between the weak scale and the KK scale $\mu_{\rm IR}$. In fact, EWSB is generic, except that in most of parameter space it is characterized by $s_h = 1$, which is not phenomenologically acceptable. The sensitivity shown in Fig. 3 is associated with the requirement $0 < s_h < 1$. Our observation is that all of this sensitivity is actually associated with getting the correct top mass (which in these scenarios is related in a relatively complicated manner to the fundamental parameters of the model), rather than with the LEP bound on the Higgs mass, which as Fig. 2 shows is easily satisfied in these scenarios.

IV. DARK MATTER IN OTHER MODELS WITH WARPED EXTRA DIMENSIONS

In the previous section, we showed how a very simple extension of a minimal composite Higgs model in warped extra dimensions successfully accounts for the observed DM relic abundance, while leading to a nontrivial connection with the physics of EWSB and EW constraints. We now briefly show that our prescription can be easily implemented in essentially any model with warped extra dimensions.

A. RS model with bulk gauge and fermion fields

This is the simplest model in which our mechanism can be applied. We will see that it is possible to get the correct DM relic density, although some fine-tuning is likely required. The bulk gauge symmetry is taken to be $SU(3)_c \times SU(2)_L \times U(1)_{X_1} \times U(1)_{X_2}$ with the Higgs field localized on or near the IR brane. The SM $U(1)$ hypercharge factor is identified with the even linear combination $U(1)_Y = U(1)_{X_+}$. The DM candidate X_- is the first KK mode of the 5D odd combination, Eq. (2.4), and has a mass given by Eq. (2.5), $m_{X_-} \approx \sqrt{2/kL}\,\mu_{\rm IR} \approx 0.24\mu_{\rm IR}$, where we have used $kL \sim \log(M_P/\text{TeV}) \approx 34$. Assuming no brane kinetic terms, the IR scale in this model must obey $\mu_{\rm IR} \gtrsim 3$ TeV [44] in order to be consistent with the EW precision measurements.[13] The annihilation rate of X_- is again fixed by the 4D coupling $\tilde{g}$ between X_-, the lightest $\mathbf{Z}_2$-odd fermion, $\psi_-^{(1)}$, and the SM zero-mode field $\psi_+^{(0)}$, and their masses. A simple computation shows that $\tilde{g} \lesssim Yg'$, with g' and Y the SM hypercharge coupling and hypercharge quantum number of $\psi_+^{(0)}$, respectively. The $\mathbf{Z}_2$-odd fermions arise as explained in Sec. II by doubling a subset of the (SM) fermion fields. These must be chosen to have a localization parameter $|c| < 1/2$, so that the resulting $\mathbf{Z}_2$-odd fields are heavier than X_-. In scenarios that explain the fermion mass hierarchies by fermion localization, this leaves as natural candidates the quarks in the third generation. The self-annihilation rate $\sigma(X_-X_- \to \psi_+^{(0)}\psi_+^{(0)})$ is too small to give the correct relic density Ωh^2, which is correspondingly too high. However, the DM relic density can be lowered to the observed level provided coannihilation processes with the colored quarks $\psi_-^{(1)}$ are important. This requires $\psi_-^{(1)}$ and X_- to be fairly degenerate, and hence $|c|$ to be very close (from below) to $1/2$. It turns out to be hard to take $c_{q_L} \simeq 1/2$ or $c_{t_R} \simeq -1/2$, because in order to get the correct 4D top Yukawa coupling one is forced to increase so much the 5D top Yukawa coupling that it would enter the strong coupling regime [3]. The alternative is to double the right-handed bottom quark only, and take $c_{b_R} \simeq -1/2$. In this case, other scattering processes become important, namely, $\sigma(X_-b_{R-} \to b_R g)$, $\sigma(b_{R-}\bar{b}_{R-} \to gg)$ and $\sigma(b_{R-}\bar{b}_{R-} \to q\bar{q})$. Given enough degeneracy between X_- and b_{R-}, the relic density of X_- can match the observation. For instance, for $m_{X_-} = 750\ (500)$ GeV, which corresponds to $\mu_{\rm IR} \simeq 3\ (2)$ TeV (see footnote [13]), one requires $c_{b_R} \simeq -0.496\ (-0.495)$. In terms of mass splittings, one gets $\Delta \equiv (m_{b_{R-}} - m_{X_-})/m_{X_-} \simeq 6\ (9)\%$. This is not a fully satisfactory scenario due to the moderate tuning needed (and the lack of independent motivation for the choice of parameters), but it shows how this idea can be successfully implemented even in the simplest 5D warped model.

By relaxing the explanation of hierarchical Yukawa couplings due to the fermion localization one can envisage a different scenario, where all (light) SM fermions share the same profile in the extra dimension. Such a situation occurs in Higgsless models, which is the subject of the next subsection.

[13] Allowing for the Higgs to be a bulk field with an exponential localization towards the IR brane [45] reduces this lower bound to $\mu_{\rm IR} \gtrsim 2$ TeV. Similarly, sizable IR brane kinetic terms for the gauge bosons can also decrease the corresponding bound on the masses of the KK modes significantly [46].

B. Higgsless models

Higgsless models induce EWSB by means of boundary conditions in the extra dimension [47]. In this way, the SM gauge bosons acquire their longitudinal components through the Higgs mechanism but no extra scalar degree of freedom (the Higgs) is present in the low-energy spectrum. Unitarity violations in longitudinal gauge boson scattering are delayed by the exchange of the gauge boson KK excitations up to the cutoff of the theory. Recently, using ideas borrowed from [3,4], the first five-dimensional Higgsless model roughly compatible with EW precision data at tree level has been presented [48].[14] A crucial ingredient is the delocalization of the (LH) light fermions [50], that have a common localization parameter close to the conformal point $c_L \lesssim 1/2$. This means that we can double the whole (LH) fermionic spectrum, following the prescription described in Sec. II, with the corresponding increase in the number of open channels for the DM particle to annihilate. Furthermore, the low IR scale favors a stronger annihilation cross section and naturally produces the right order of magnitude for the relic abundance. Our starting point is the model of Ref. [48], in which $c_L = 0.46$. In this case, the bulk gauge group is $SU(2)_L \times SU(2)_R \times U(1)_{X_1} \times U(1)_{X_2}$, with $U(1)_{B-L} = U(1)_{X_+}$ the even combination of X_1 and X_2. The smaller warp factor and lower IR scale in this model lead to a relatively light DM candidate, with mass $m_{X_-} \sim 0.4\mu_{\rm IR} \sim 114$ GeV. Doubling the whole LH light spectrum leads to a too large annihilation cross section, mostly due to the larger charge of the leptonic fields under the $U(1)_{B-L}$ group, whereas doubling only the light LH quarks results in a cross section that is a bit too small. As an example, doubling only one LH lepton doublet, we obtain $\Omega h^2 \sim 0.07$. This is impressively close to the observed value, considering that we have taken identical values for all the parameters, as in Ref. [48].

V. PHENOMENOLOGY OF THE DARK MATTER SECTOR

A. Collider phenomenology

The collider signatures of our construction share common qualitative features with other models of new physics with stable particles. New states are produced in pairs and (cascade) decay to SM particles and the LOP, which is perceived as missing energy in the detector. The specific details of the spectrum of NLOP induce, however, significant differences at the quantitative level.

In order to be more specific, we will discuss the phenomenology of the GHU model described in Sec. III. We study, as an interesting and representative example, the case with $c_u > 0$. The light $\mathbf{Z}_2$-odd spectrum consists of the LOP with a mass $m_{X_-} \sim 300$–400 GeV and the first KK modes of the bidoublet component of ξ_u^-, that contain two quarks of charge $2/3$, one of charge $5/3$ and one of charge $-1/3$. We will denote these quarks as t', q^u, χ^u and q^d, respectively, and, generically, as ψ. They are degenerate, with a mass $m_\psi - m_{X_-} \sim 0.15 m_{X_-}$, except for small EWSB effects that make one of the charge $2/3$ quarks (t') slightly lighter.

Vectorlike quarks are pair-produced at the CERN LHC via the QCD interactions with a model-independent cross section that depends only on the mass of the quark [51],

$$\sigma_{pp\to Q\bar{Q}} \sim 15\ (1.5)\ \text{pb}, \quad \text{for } m_Q \sim 400\ (600)\ \text{GeV}. \tag{5.1}$$

The distinctive feature is the high degree of degeneracy between the NLOP and the LOP, which forbids the natural cascade decay through a top quark, leaving decays into light jets and missing energy (the LOP) as the main signature. The charge $5/3$ quark cannot directly decay into the LOP and SM particles, and therefore undertakes a cascade decay through an off-shell W^* to t', which then decays to jets and missing energy.

The decay width for the two-body decays (kinematically allowed for q^d and, through intergenerational mixing for t' and q^u) is given, to leading order in the mass difference, by (the inverse of) Eq. (3.15)

$$\Gamma(\psi \to jX_-) \approx \frac{3\lambda^2}{8\pi}\Delta^2 m_\psi \approx (4\times 10^{-6}\ \text{GeV})\left(\frac{\lambda}{0.002}\right)^2\left(\frac{\Delta}{0.15}\right)^2\frac{m_\psi}{460}, \tag{5.2}$$

where $j = u, c, b$, the relevant coupling is denoted with λ, ψ stands here for any of t', q^u and q^d, and m_ψ is measured in GeV. For the numerical result we have replaced the different parameters with typical values for the charge $2/3$ quarks [we have assumed intergenerational mixing in the up sector to be of the order of the corresponding Cabbibo-Kobayashi-Maskawa matrix elements $\lambda \sim V_{ub,cb}\tilde{g}/\sqrt{2} \lesssim 0.2 \times (10^{-2}$–$10^{-3})$]. In the case of q^d there is no intergenerational mixing suppression ($\lambda = \tilde{g}$) and the width can easily be

$$\Gamma(q^d \to bX_-) \approx (10^{-1}\text{–}10^{-2})\ \text{GeV}. \tag{5.3}$$

The corresponding three-body decay for χ^u proceeds through an off-shell W^*, which can decay leptonically. In the contact interaction approximation, the partial decay width into muons is

$$\Gamma(\chi^u \to t'\mu^+\nu_\mu) = \frac{G_F^2 m_{\chi^u}^5}{192\pi^3} f(x) \approx (6\times 10^{-5}\ \text{GeV})\left(\frac{m_{\chi^u}}{500\ \text{GeV}}\right)^5\frac{f(x)}{f(0.9)}, \tag{5.4}$$

[14] Deconstructed versions of Higgsless models are more flexible than five-dimensional ones and models compatible with data, at the tree level, have been constructed [49].

where $f(x) = 1 - 8x^2 + 8x^6 - x^8 - 12x^4 \log x^2$, with $x \equiv m_{t'}/m_{\chi^u}$.

Thus, we see that the NLOP are produced with a large cross section and decay promptly, leading to the following typical signatures:

$$pp \to t'\bar{t}', q^u\bar{q}^u, q^d\bar{q}^d \to jj\not{E}_T, \tag{5.5}$$

$$pp \to \chi^u\bar{\chi}^u \to t'\bar{t}'W^*W^* \to l\nu jjjj\not{E}_T. \tag{5.6}$$

The former signature, that can benefit from a larger cross section due to the quark multiplicity, is challenging due to the lack of leptons to trigger on, and the fact that the amount of transverse missing energy is limited by the small mass difference between the NLOP and the LOP. The latter, more promising due to the presence of a leptonically decaying W, has however the problem of the extra source of missing energy (the neutrino from the W^*) and the fact that the W^* is off its mass shell and therefore its mass cannot be reconstructed. A detailed analysis, which is beyond the scope of this work, is needed to asses the trigger efficiency in accepting the signal and the best strategy to search for this new sector in models with warped extra dimensions, but the large production cross sections seem to indicate that discovery should be possible at the LHC.

Thus, although the generic collider implications of our construction share some features with other models of new physics with stable particles, the particular details of the spectrum of NLOP give a very characteristic signature, with direct decays into jets plus missing energy and, in some cases, also short cascade decays through off-shell W's. These are challenging signals at the LHC, but the large cross sections due to the low mass of the new particles and the high multiplicity should help in the discovery of these channels. One should also remember that the $\mathbf{Z}_2$-even sector of these models is also predicted to have light resonances. In the particular case we are discussing, we have a light quark doublet with hypercharge $7/6$ that will be easily observed in the early phase of the LHC [52]. The more challenging, although possible [53], discovery of the gauge boson KK excitations and the lightest particles of the $\mathbf{Z}_2$-odd sector as we have described above, should then draw a clear picture of the structure of EWSB.

B. Direct dark matter searches

Direct detection of DM particles is mostly based on detectors in which the relevant process is the scattering amplitude DM atoms $\to$ DM atoms. Since, as we have seen, X_- typically couples only to third generation quarks (the top quark in the GHU model, b_R in the RS model), its direct detection rate is expected to be too small for current and future planned experiments. We can be more quantitative and estimate the cross section $X_-N \to X_-N$, where N is a nucleon. Not surprisingly, the situation is analogous to that of UED where the DM particle is identified with the first KK mode of the 5D hypercharge gauge field, with the important difference that in our case there is no Higgs exchange and only heavy quarks Q are relevant. Following [54] and using their notation, the spin-independent cross section reads

$$\sigma_{\text{scalar}} = \frac{m_N^2}{4\pi(m_{X_-} + m_N)^2} f_N^2, \tag{5.7}$$

where $f_N = \beta_Q \langle N|\bar{Q}Q|N\rangle$ with Q top or bottom quarks, and

$$\beta_Q \simeq m_Q(Q_{X,L}^2\tilde{g}_L^2 + Q_{X,R}^2\tilde{g}_R^2)\frac{m_{X_-}^2 + m_\psi^2}{(m_{X_-}^2 - m_\psi^2)^2}, \tag{5.8}$$

with m_ψ the mass of the NLOP. A careful estimate of the nuclear matrix element $\langle N|Q\bar{Q}|N\rangle$ would require a detailed one-loop analysis, along the lines of [55]. For an order of magnitude estimate, it is however enough to use the old result [56]

$$\langle N|\bar{Q}Q|N\rangle = \frac{2}{27}\frac{m_N}{m_Q}\left(1 - \sum_{q=u,d,s} f_{T_q}^N\right), \tag{5.9}$$

where $f_{T_q}^N = \langle N|\bar{q}q|N\rangle m_q/m_N$. It is now straightforward to compute σ_{scalar}. For the GHU model we considered, by taking, say, $m_{X_-} \simeq 350$ GeV, $m_\psi \simeq 380$ GeV, $\tilde{g}_L = 0$, $\tilde{g}_R \simeq 0.25$, $Q_{X,R} = 2/3$, one has

$$\sigma_{\text{scalar}} \simeq 2 \times 10^{-10} \text{ pb}, \tag{5.10}$$

which is a value too low for current experiments and would require new experiment proposals, such as supercryogenic dark matter search [57]. Because of the higher value of m_{X_-}, σ_{scalar} is even smaller in the RS model with doubled b_R considered in Sec. IVA. In both models, due to the denominator term in Eq. (5.8), σ_{scalar} can become sizable only for extreme degenerate cases in which $m_{X_-} \simeq m_\psi$.

In the Higgsless model, the situation is different, since one might also have direct couplings of X_- with light quarks. In addition, X_- is lighter, $m_{X_-} \sim 100$ GeV, and hence DM direct detection seems more promising. However, in the specific model of [48], σ_{scalar} is still suppressed due to the low values of the charges, $Q_{X,L} = 1/6$ ($Q_{X,R} = 0$), resulting in a cross section of the same order of magnitude as (5.10).

VI. A COMMENT ON ANOMALIES

We have assumed so far that the $\mathbf{Z}_2$ exchange symmetry is an exact symmetry of the theory, namely, that no quantum corrections can possibly violate it. We show here that the exchange symmetry is exact by noticing that the CS terms that are required by gauge invariance are always $\mathbf{Z}_2$-even and hence invariant. This is actually expected, since the $\mathbf{Z}_2$ symmetry is a global symmetry which has nothing to do with parity, the discrete symmetry typically broken by anomalies. For simplicity, we will focus our attention on the simplest RS scenario with fermion and

gauge bulk fields analyzed in Sec. IVA, but the main results remain valid also for the more refined GHU model of Sec. III.

The bulk gauge group is $G = SU(3)_c \times SU(2)_L \times U(1)_{X_1} \times U(1)_{X_2}$, broken to $SU(3)_c \times SU(2)_L \times U(1)_Y$ at the IR brane and fully unbroken at the UV brane. The 5D fermion spectrum consists of massive Dirac fermions, one for each SM fermion, with $(++)$ or $(--)$ b.c., depending on the chirality of the SM fermion. They have charge $(\frac{1}{2}Y, \frac{1}{2}Y)$ under $U(1)_{X_1} \times U(1)_{X_2}$, with Y the corresponding SM hypercharge for the given fermion field, while the 5D bottom fermion fields ψ_{b_1} and ψ_{b_2} have charges $(-1/3, 0)$ and $(0, -1/3)$. Although the 4D massless fermion spectrum of the model is anomaly-free by construction, being identical to the SM spectrum, the 5D theory needs CS terms to restore 5D gauge invariance fully, because localized anomalies (globally vanishing in 4D once integrated over the internal space) appear at the UV and IR branes (see [58] for a review).[15] Recall that the warping does not alter the localization pattern of anomalies, which is then as in flat space [59]. It is extremely useful to also recall that the form of a localized anomaly at a boundary is fully determined by the "effective" chiral spectrum which is found there by neglecting the b.c. at the other end point, which is equivalent to sending the other boundary to infinity (see e.g. [58] for a derivation of this result). Let us consider the UV brane, where both $U(1)$ factors are unbroken, and focus on the possible anomalies involving the gauge field X_-. All SM fermions are neutral under $U(1)_{X_-}$, with the exception of ψ_{b_1} and ψ_{b_2}, which have opposite charges $-1/3$ and $+1/3$. Correspondingly, all $U(1)^3_{X_-}$, $U(1)_{X_-}U(1)^2_Y$, $SU(3)_c U(1)_{X_-}$ and mixed $U(1)_{X_-}$-gravitational anomalies trivially vanish at the UV brane. At the IR brane, no anomalies involving $U(1)_{X_-}$ can appear, since the gauge field X_- vanishes there. It is not difficult to compute all other localized anomalies. One finds that the doubling procedure induces pure $SU(3)_c$, $U(1)^3_Y$ and mixed $SU(3)_c U(1)_Y$, $U(1)_Y$-gravitational anomalies at the UV and IR brane, as well as a $U(1)_Y U(1)^2_{X_-}$ anomaly at the UV brane. All these anomalies are cancelled by suitable 5D CS terms, which involve either 0 (the former) or 2 (the latter) gauge fields X_-.[16] Consequently, all CS terms are $\mathbf{Z}_2$-even, as anticipated. A similar result is found for the GHU model of Sec. III.

[15] In this simple example, localized anomalies appear only due to the doubling we have performed. The original model is fully anomaly-free since the SM anomaly cancellation applies also to the localized terms.

[16] Possible modifications to the wave functions of gauge fields induced by such CS terms can be safely neglected, being one-loop suppressed.

VII. DISCUSSION AND CONCLUSIONS

In this paper we have proposed a generic construction that allows one to endow given models with a DM candidate. This is achieved through an extension in which the model acquires a $\mathbf{Z}_2$ exchange symmetry. The lightest $\mathbf{Z}_2$-odd particle is then absolutely stable.

We have considered several models with warped extra dimensions. Although these scenarios are well-motivated extensions of the SM, explaining both the Planck-weak scale hierarchy as well as the flavor structure of the SM, they do not contain, generically, stable particles that can account for the observed DM component of the Universe. We have shown that our mechanism can easily solve this deficiency.

We have paid special attention to a class of warped scenarios that is particularly appealing: GHU/composite Higgs scenarios. In this case, the $\mathbf{Z}_2$ structure responsible for the stability of the DM candidate is tightly connected to the physics that leads to the dynamical breaking of the EW symmetry. As in supersymmetry, the dark matter mass and couplings are intimately connected to the EW scale. In fact, not only does our construction not introduce new parameters, but there is a further sense in which it can be considered minimal. As was emphasized in the main text, the physics of EWSB in such models crucially depends on certain fields that have two properties: they are fermionic fields without zero modes and, through their strong connection to the top sector, they give a significant—in fact, crucial—contribution to the Higgs potential. This is precisely the sector that gives rise to the $\mathbf{Z}_2$-odd particles that can lead to a realistic dark matter candidate. As a result, the $\mathbf{Z}_2$-odd sector, through its contribution to the Higgs potential, plays a key role in the realization of an EWSB vacuum with the desired physical properties. As explained in detail in the main text, the effects due to the $\mathbf{Z}_2$-odd sector go in the direction of alleviating the constraints imposed by low-energy measurements. The picture that emerges is rather compelling: the observed DM relic abundance and the very precise measurements of the EW observables at LEP and Stanford Linear Accelerator Center Linear Collider point to a *common* region in parameter space. This region is characterized by several fermionic resonances nearly degenerate with the DM candidate (a spin-1 particle), which in turn is predicted to have a mass in the 300–500 GeV range.

We have also pointed out that although the GHU scenarios (with or without DM) present a sensitivity of order 1% or worse with respect to microscopic parameters (larger than what naive considerations would indicate), this sensitivity disappears once the top mass measurement is imposed. Thus, the moderate sensitivity of order a percent, that is present in virtually every extension of the SM that has any relation to the physics of EWSB acquires a new twist: it indicates an intrinsic difficulty in accommodating a heavy top. By contrast, once the top mass is fixed to a

value of order the EW scale, the Higgs mass easily satisfies the LEP bound, while typically lying below 170 GeV or so.

Regarding the phenomenological implications of our construction, the low scale predicted for the new $\mathbf{Z}_2$-odd sector and, in particular, new vectorlike quarks, guarantees large production cross sections. Because of the particular features of the NLOP spectrum, which is very degenerate with the LOP, the most common signature will be jets plus missing energy accompanied in some cases by the semileptonic decays of a pair of off-shell W^*. These are challenging signatures that will require dedicated analysis. The large production cross sections and the information coming from the easier channels in the $\mathbf{Z}_2$-even sector should however be sufficient to guarantee a discovery of the DM sector at colliders. We have also seen that DM direct detection is not very promising in present or near future experiments, due to the fact that couplings to light valence quarks are suppressed by intergenerational mixing, leading to very small cross sections.

ACKNOWLEDGMENTS

We thank P. Batra, G. Cacciapaglia, B. Dobrescu, J. Hubisz, R. Iengo, K. C. Kong, J. Lykken, A. Romanino, V. S. Rychkov and P. Ullio for useful discussions. This work was partially supported by the European Community's Human Potential Programme under Contract No. MRTN-CT-2004-005104. The work of G. P. was partially supported by the European Union 6th framework program MRTN-CT-2004-503069 "Quest for unification", MRTN-CT-2004-005104 ForcesUniverse, MRTN-CT-2006-035863 UniverseNet and SFB-Transregio 33 "The Dark Universe" by Deutsche Forschungsgemeinschaft (DFG). E. P. was supported by the DOE under Grant No. DE-FG02-92ER-40699. J. S. was partially supported by the U.S. DOE under Contract No. DE-AC02-07CH11359 and by SNSF under Contract No. 200021-117873. M. S. thanks Fermilab and J. S. the Aspen Center for Physics for hospitality during the early stages of this work.

APPENDIX A: THE MCHM$_5$ WITH DARK MATTER

In this section we summarize the model of GHU that was analyzed in the main text. The model has an $SO(5) \times U(1)_{X_1} \times U(1)_{X_2}$ bulk gauge symmetry, with a discrete symmetry under which the two $U(1)$ factors are exchanged. The $\mathbf{Z}_2$-even sector is identical to the MCHM$_5$ of Ref. [25]. The $SO(5)/SO(4)$ directions are broken on both branes by choosing $(-,-)$ boundary conditions for the μ components

$$A_\mu^{\hat{a}}(-,-), \tag{A1}$$

where $\hat{a} = 1, \ldots, 4$ runs over the $SO(5)/SO(4)$ indices. The corresponding components along the extra dimension $A_5^{\hat{a}}$ (which are four-dimensional scalars) have zero modes that transforms as a bidoublet of $SO(4) \sim SU(2)_L \times SU(2)_R$ and are identified as the SM Higgs doublet. The μ components of the remaining gauge fields have the following b.c.:

$$W_L^a \sim (+,+), \qquad B \sim (+,+), \tag{A2}$$

$$W_R^b \sim (-,+), \qquad Z' \sim (-,+), \tag{A3}$$

where $a = 1, 2, 3$, $b = 1, 2$, the L and R indices correspond to the $SU(2)_L \times SU(2)_R$ decomposition of $SO(4)$, and

$$B = \frac{g_{5X} W_R^3 + g_5 X_+}{\sqrt{g_5^2 + g_{5X}^2}}, \qquad Z' = \frac{g_5 W_R^3 - g_{5X} X_+}{\sqrt{g_5^2 + g_{5X}^2}}. \tag{A4}$$

Here we have defined $X_\pm = (X_1 \pm X_2)/\sqrt{2}$, and $X_{-\mu}$ satisfies $(+,-)$ b.c. Also, $g_{5X_1} = g_{5X_2} = \sqrt{2} g_{5X}$.

The SM quarks are embedded in bulk fermions transforming in the fundamental representation of $SO(5)$, $\mathbf{5} = (2,2) \oplus (1,1)$ with X_+ charge $2/3$ and $-1/3$ for the up and down sectors, respectively. The odd fields couple as in Eq. (2.3). The b.c. are as follows:

$$\xi_{q_1} = \begin{bmatrix} (2,2)_L^{q_1} = \begin{bmatrix} q'_{1L}(-+) \\ q_{1L}(++) \end{bmatrix} & (2,2)_R^{q_1} = \begin{bmatrix} q'_{1R}(+-) \\ q_{1R}(--) \end{bmatrix} \\ (1,1)_L^{q_1}(-,-) & (1,1)_R^{q_1}(+,+) \end{bmatrix},$$

$$\xi_u^+ = \begin{bmatrix} (2,2)_L^u(+-) & (2,2)_R^u(-+) \\ (1,1)_L^u(-+) & (1,1)_R^u(+-) \end{bmatrix}, \qquad \xi_u^- = \begin{bmatrix} (2,2)_L^{u^-}(+-) & (2,2)_R^{u^-}(-+) \\ (1,1)_L^{u^-}(-+) & (1,1)_R^{u^-}(+-) \end{bmatrix}, \tag{A5}$$

$$\xi_{q_2} = \begin{bmatrix} (2,2)_L^{q_2} = \begin{bmatrix} q_{2L}(++) \\ q'_{2L}(-+) \end{bmatrix} & (2,2)_R^{q_2} = \begin{bmatrix} q_{2R}(--) \\ q'_{2R}(+-) \end{bmatrix} \\ (1,1)_L^{q_2}(-,-) & (1,1)_R^{q_2}(+,+) \end{bmatrix}, \qquad \xi_d = \begin{bmatrix} (2,2)_L^d(+-) & (2,2)_R^d(-+) \\ (1,1)_L^d(-+) & (1,1)_R^d(+-) \end{bmatrix}.$$

We have displayed the field content according to their $SO(4)$ decomposition, and $+$ and $-$ represent, respectively,

Neumann or Dirichlet boundary conditions at the corresponding brane. Note that the choice of parities above seems to allow for two SM doublet zero modes per generation, coming from q_{1L} and q_{2L}. It is actually only the symmetric combination $(q_{1L} + q_{2L})/\sqrt{2}$ that has a zero mode, the odd combination being coupled to a UV-localized chiral fermion with a large mass. The $O(4) \times U(1)_X$ symmetry at the IR brane allows for the following mass mixing terms:

$$m_u \overline{(2,2)}_L^{q_1}(2,2)_R^u + M_u \overline{(1,1)}_R^{q_1}(1,1)_L^u + m_d \overline{(2,2)}_L^{q_2}(2,2)_R^d + M_d \overline{(1,1)}_R^{q_2}(1,1)_L^d + \text{H.c.} \quad \text{(A6)}$$

Notice that the localized mass terms do not involve the odd fields in ξ_u^-. Thus, neglecting intergenerational mixing, we have a total of eight parameters per quark generation, four bulk masses, denoted in units of the bulk curvature k by c_{q_1}, c_{q_2}, c_u and c_d (the exchange symmetry forces $c_{u^-} = c_u$), and four mass terms $m_{u,d}$, $M_{u,d}$. The first two generations have a negligible effect on EWSB and, for the third generation, as long as $c_{q_1} < 1/2$, $c_{q_1} < c_{q_2}$, the two multiplets related to the bottom (ξ_{q_2}, ξ_d) do not play any significant role either. We are therefore left with four relevant parameters c_{q_1}, c_u, m_u and M_u. Note however that there is a phenomenological constraint on the value of c_d. The reason is that, due to the chosen boundary conditions, the component $(1,1)^d$ becomes ultralight for $c_d \lesssim -1/2$ [18], easily violating limits from direct production at the Tevatron [60].

APPENDIX B: THE HIGGS POTENTIAL

The one-loop Higgs potential in 5D warped models does not admit a simple analytic expression, which is related to the difficulty in deriving an explicit form for the KK mass spectrum and Higgs interactions for the relevant fields. A useful tool to derive at least an implicit but relatively compact form for the potential is achieved by using the gauge-fixing outlined in [61] in an holographic approach [62]. In this way, the Higgs potential is simply obtained by a rotation of the 4D holographic fields only (see [61] for details). The Higgs potential in our model is actually the same as the one considered in [25], the only difference being the presence of the $\mathbf{Z}_2$-odd $SO(5)$ multiplet ξ_u^-. The latter field, interestingly enough, leads to a Higgs contribution which has opposite sign with respect to that of 5D fermions admitting chiral zero modes. Like gauge fields, they contribute positively to the Higgs potential, pushing the minimum towards zero. In order to simplify the discussion, let us consider a simple 5D model with $SU(2)$ gauge symmetry broken to $U(1)$ by boundary conditions. The contribution to the "Higgs" potential given by two 5D fermion doublets $\Psi_\pm$ whose left-handed components satisfy the boundary conditions

$$\Psi_L^+ = \begin{pmatrix} \psi_L^u(++) \\ \psi_L^d(--) \end{pmatrix}, \qquad \Psi_L^- = \begin{pmatrix} \psi_L^u(+-) \\ \psi_L^d(-+) \end{pmatrix}, \quad \text{(B1)}$$

modulo an irrelevant constant term, can be written as

$$V_\pm(h) = -2 \int \frac{d^4p}{(2\pi)^4} \log[1 \pm c_{2h} \Pi(p, m_\pm)]. \quad \text{(B2)}$$

In Eq. (B2), $\pm$ stands for the contributions of Ψ^+ and Ψ^-, respectively, p is an Euclidean momentum and $c_{2h} = \cos(2h/f_h)$. All the nontrivial information on the mass spectrum is encoded in the form factor $\Pi(p, m_\pm)$, with $p = \sqrt{p_\mu p^\mu}$ and $m_\pm$ the bulk 5D mass terms. If $|\Pi(p, m_\pm)| < 1$ over the whole integration region, then one can expand the log term in Eq. (B2), which clearly shows the opposite contribution to the potential given by the two 5D fermion fields. One has

$$\Pi(p, m) = \left[\frac{G_{--}(c)}{G_{-+}(c)} - \frac{G_{+-}(c)}{G_{++}(c)}\right]\left[\frac{G_{--}(c)}{G_{-+}(c)} + \frac{G_{+-}(c)}{G_{++}(c)}\right]^{-1}, \quad \text{(B3)}$$

where $G_{\pm,\pm}(c) = G_{\pm,\pm}(c, p, z_{\text{IR}}, z_{\text{UV}})$ are a combination of the Bessel functions J and Y:

$$G_{\eta,\eta'}(c, p, z_1, z_2) = J_{c+\eta 1/2}(ipz_1) Y_{c+\eta' 1/2}(ipz_2) - Y_{c+\eta 1/2}(ipz_1) J_{c+\eta' 1/2}(ipz_2), \quad \text{(B4)}$$

where $\eta, \eta' = \pm$, and $c = z_{\text{UV}} m$ is the usual dimensionless mass term in warped space. It is not difficult to check that $|\Pi(p, m_\pm)| \leq 1$; it exponentially vanishes when $p \to \infty$ and reaches its maximum value 1 just at the origin $p = 0$.[17]

Let us now turn to the actual Higgs potential in our model, which is complicated by the presence of localized IR mass terms and a nontrivial gauge symmetry breaking pattern. The most relevant fields contributing to the potential are the gauge fields and the $SO(5)$ multiplets $\xi_u^\pm$, ξ_d, ξ_{q_1} and ξ_{q_2}. In the holographic approach, these contributions are encoded in the holographic gauge fields W and Z, the bottom and top quarks, and by a holographic $\mathbf{Z}_2$-odd-fermion component of ξ_u^-.

The gauge field contribution reads (in the absence of any localized IR or UV terms)

$$V_g(h) = \frac{3}{2} \int \frac{d^4p}{(2\pi)^4} \left[2 \log\left(1 + s_h^2 \frac{\Pi_- - \Pi_+}{2\Pi_+}\right) + \log\left(1 + s_h^2 \frac{\Pi_- - \Pi_+}{2\Pi_+} \frac{2}{(1 + \cos 2\theta_W)}\right)\right], \quad \text{(B5)}$$

where θ_W is the SM weak mixing angle and

$$\Pi_\pm = \frac{G_{\mp-}(1/2)}{G_{\mp+}(1/2)}, \quad \text{(B6)}$$

[17] A similar result holds in flat space where $\Pi(p, m) = -(p^2 + m^2)/(m^2 + p^2 \cosh(2L\sqrt{p^2 + m^2}))$, with L being the length of the segment.

in terms of the functions defined in Eq. (B4). In Eq. (B5), the first and second log terms correspond to the holographic W and Z contributions, respectively.

Let us now consider the fermion contribution to the Higgs potential. Since by symmetry no IR mass terms can be introduced for ξ_u^-, whose components satisfy boundary conditions of the $(+-)/(-+)$ type, its contribution to the potential is given by $V_-(h)$ in Eq. (B2), which can be rewritten (again, modulo constant terms) as

$$V_f^-(h) = -2N_c \int \frac{d^4p}{(2\pi)^4} \log\left[1 + s_h^2 \frac{\Pi_1}{2\Pi_0}\right], \tag{B7}$$

where $N_c = 3$ is the QCD color factor and

$$\begin{aligned} \Pi_0 &= -\frac{G_{-+}(c_u)}{G_{--}(c_u)}, \\ \Pi_1 &= -2\left(-\frac{G_{-+}(c_u)}{G_{--}(c_u)} + \frac{G_{++}(c_u)}{G_{+-}(c_u)}\right). \end{aligned} \tag{B8}$$

The holographic bottom and top quark contributions are more involved. The top contribution can be written as

$$\begin{aligned} V_{\rm top}(h) = -2N_c \int \frac{d^4p}{(2\pi)^4} \log\Bigg[&\left(1 + s_h^2 \frac{\Pi_1^u}{2\Pi_0^u}\right)\left(1 + s_h^2 \frac{\Pi_1^{q_1}}{2\Pi_0^q}\right) \\ &- s_h^2 c_h^2 \frac{(M_1^u)^2}{2\Pi_0^u \Pi_0^q}\Bigg], \end{aligned} \tag{B9}$$

in terms of the following form factors:

$$\begin{aligned} \Pi_0^u &= -\frac{N^+_{q_1,u}(1/M_u)}{D_{q_1,u}(1/M_u)}, \\ \Pi_1^u &= -2\left[-\frac{N^+_{q_1,u}(1/M_u)}{D_{q_1,u}(1/M_u)} + \frac{N^+_{q_1,u}(m_u)}{D_{q_1,u}(m_u)}\right], \\ \Pi_0^q &= \frac{N^-_{q_1,u}(m_u)}{D_{q_1,u}(m_u)} + \frac{N^-_{q_2,d}(m_d)}{D_{q_2,d}(m_d)}, \\ \Pi_1^{q_1} &= -\frac{N^-_{q_1,u}(m_u)}{D_{q_1,u}(m_u)} + \frac{N^-_{q_1,u}(1/M_u)}{D_{q_1,u}(1/M_u)}, \\ M_1^u &= \frac{4}{\pi^2 p^2 z_{\rm IR} z_{\rm UV}}\left(\frac{m_u}{D_{q_1,u}(m_u)} - \frac{1/M_u}{D_{q_1,u}(1/M_u)}\right), \end{aligned} \tag{B10}$$

with

$$\begin{aligned} N^\pm_{i,j}(M) &= G_{-\pm}(c_i)G_{+\pm}(c_j) + M^2 G_{+\pm}(c_i)G_{-\pm}(c_j), \\ D_{i,j}(M) &= G_{-+}(c_i)G_{+-}(c_j) + M^2 G_{++}(c_i)G_{--}(c_j). \end{aligned} \tag{B11}$$

In the above formulas, m_u and M_u are dimensionless IR brane mass terms (see Appendix A). The bottom quark contribution is also given by Eq. (B9), provided one makes the substitutions $c_{q_1} \leftrightarrow c_{q_2}$, $c_u \leftrightarrow c_d$, $m_u \leftrightarrow m_d$, $M_u \leftrightarrow M_d$ in Eqs. (B9) and (B10).

It is useful to consider various limits for the IR brane mass terms. When $m_u \to 0$, $M_u \to 0$, the form factor M_1^u vanishes and the potential splits in the two contributions given by ξ_u^+ and ξ_{q_1,q_2}. As expected, in this limit the contribution given by ξ_u^+ reduces to that of ξ_u^-, with $\Pi_0^u \to \Pi_0$, $\Pi_1^u \to \Pi_1$, with Π_0 and Π_1 given in Eq. (B8). In the opposite limit, $m_u \to \infty$, $M_u \to \infty$, the contribution given by ξ_u^+ turns into that of a fermion with $(++)/(--)$ boundary conditions, and is given by $V_f^+(h)$ in Eq. (B2). This is again expected, since the large IR brane mass terms effectively change the boundary conditions of the fermions on the IR brane. In the limits in which $M_u \to \infty$, $m_u \to 0$ or vice versa, $\Pi_1^u \to 0$, $M_1^u \to 0$, and hence ξ_u^+ does not contribute at all to the potential. As far as ξ_{q_1,q_2} are concerned, one should recall that bottom and top quarks are distributed in both multiplets ξ_{q_1} and ξ_{q_2} and that a localized UV right-handed fermion doublet is necessary to get rid of an unwanted zero-mode left-handed doublet [25]. Such a localized field implies that the contributions of ξ_{q_1} and ξ_{q_2} are entangled also in the limit of vanishing or very large IR brane terms. That is why Π_0^q in Eq. (B10) depends on both c_{q_1,q_2}, $c_{u,d}$ and $m_{u,d}$. Notice, however, that even in this case, if $M_u \to \infty$, $m_u \to 0$ or vice versa, $\Pi_1^{q_1}$ vanishes, so that the whole top contribution to the potential vanishes in this limit. Such a result is particularly clear in the approach followed here, where the Higgs dependence of the holographic Lagrangian is obtained by a $SO(5)$ rotation of the 4D holographic fields. The rotation gives rise to Higgs-dependent terms when $SO(5)$ is broken at the IR brane by boundary conditions. In the limit $M_u \to \infty$, $m_u \to 0$ or vice versa, the singlet and the bidoublet components of the $SO(5)$ multiplets ξ_u^+, ξ_{q_1} and ξ_{q_2} have the same boundary conditions at the IR brane, implying $SO(5)$ invariant boundary conditions and hence no couplings of such fermions with the Higgs. Actually, there is a whole one-dimensional family of boundary conditions, when $m_u = 1/M_u$, for which $\Pi_1^u = \Pi_1^{q_1} = M_1^u = 0$, as is clear from Eq. (B10). Needless to say, similar results hold when considering the IR brane terms m_d and M_d.

The total one-loop Higgs potential is finally given by

$$V_{\rm Tot}(h) = V_g(h) + V_{\rm top}(h) + V_{\rm bottom}(h) + V_f^-(h). \tag{B12}$$

APPENDIX C: THE TRILINEAR COUPLINGS

The holographic approach, used in the previous appendix to derive the effective Higgs potential, can also be efficiently applied to the computation of the trilinear couplings $\tilde{g}_L$ and $\tilde{g}_R$ of the DM candidate X_- with the third generation quarks and the $\mathbf{Z}_2$-odd fermions. As explained in the main text, these couplings are an essential ingredient to compute the DM relic abundance.

For simplicity, we neglect EWSB effects, which introduce only a slight change ($\lesssim$ a few%) in the computation of the DM relic abundance, an accuracy that we have no interest in achieving. Starting from Eqs. (3.4) and (3.5), our aim is to extract the trilinear couplings $\tilde{g}_R \bar{t}_R \not{X}_- \psi_{-,R}$ (for $c_u < 0$) and $\tilde{g}_L \bar{t}_L \not{X}_- \psi_{-,L}$ (for $c_u > 0$) where $\psi_{-,R}$ is the

right-handed component of the NLOP singlet state and $\psi_{-,L}$ is the left-handed component of the NLOP field in the bidoublet coupled to the top. In the holographic approach, $\tilde{g}_{L/R}$ are obtained by writing the bulk-to-boundary propagators for the holographic fields $t_{L/R}$, $\psi_{-,L/R}$ and X_- and integrating the vertices (3.4) and (3.5) over the compact space, taking care of normalization factors required to define canonically normalized fields. We can consider the cases $c_u > 0$ and $c_u < 0$ at the same time. The (t_L, t_R) system can be described by choosing as holographic degrees of freedom the UV values of the LH components of the ξ_{q_1} (and ξ_{q_2}) multiplet and the RH ones of the ξ_u^+ field (for $m_u \neq 0$). In this way we obtain the quadratic holographic Lagrangian

$$\mathcal{L} = \bar{t}_L \frac{\not{p}}{p} \frac{\Pi_0^q}{z_{\rm UV}} t_L + \bar{t}_R \frac{\not{p}}{p} \frac{\Pi_0^u}{z_{\rm UV}} t_R, \tag{C1}$$

with $p = \sqrt{p_\mu p^\mu}$ and p_μ a Minkowskian momentum and the form factors Π_0^q and Π_0^u are as in Eq. (B10) but with $p \to -ip$.[18]

The holographic fields are not mass eigenstates but rather a superposition of all the states in the 4D KK tower. As a consequence, we need some care to extract the couplings of the mass eigenstates from the holographic Lagrangian. To do this we use the fact that the holographic fields coincide with the (noncanonically normalized) mass eigenstates when we put them on mass shell. This means that we can obtain the couplings of the KK states by simply computing the holographic couplings on-shell, provided we also find the correct normalization factors for the fields.

For the top field, the wave functions of the relevant on-shell (i.e. $p = 0$) components along the ξ_u^+ multiplet are given by

$$\begin{cases} \xi^+_{u,L}(z) = -m_u z^{2-c_u} z_{\rm IR}^{c_u - c_{q_1}} z_{\rm UV}^{c_{q_1} - 5/2} t_L \equiv f_L^+(z) t_L, \\ \xi^+_{u,R}(z) = \frac{1}{\sqrt{z_{\rm UV}}} \left(\frac{z}{z_{\rm UV}}\right)^{2+c_u} t_R \equiv f_R^+(z) t_R. \end{cases} \tag{C2}$$

To find the correct normalization factors $Z^+_{L,R}$, we must require that the action have the canonical form for massless fields in a series expansion in p around the on-shell momentum. The L and R normalization factors are thus given by

$$(Z^+_{L,R})^2 = \lim_{p\to 0} \frac{1}{z_{\rm UV}} \frac{\Pi_0^{q,u}}{p} = \lim_{p\to 0} \frac{1}{z_{\rm UV}} \frac{\partial \Pi_0^{q,u}}{\partial p}. \tag{C3}$$

Because of the absence of zero modes, the holographic description of the $\mathbf{Z}_2$-odd fields is more involved, since the action diverges for $p \to 0$. Nevertheless we can still use the holographic approach by a suitable expansion around the on-shell momentum $p = m_{\rm odd}$, where $m_{\rm odd}$ is a mass eigenvalue.

The NLOP states that couple to t_R and t_L, $\psi_{-,R}$ and $\psi_{-,L}$, are contained in the multiplet ξ_u^- as in Eq. (A5), namely, $\xi_R^- = (1,1)_R^{u-}$ and the relevant component of $(2,2)_L^{u-}$, that we denote by ξ_L^-. Both fields satisfy $(+-)$ b.c., so that we can choose as holographic fields the UV values of the corresponding components: $\psi_R^- \equiv \sqrt{z_{\rm UV}} \xi_R^-(z_{\rm UV})$ and $\psi_L^- \equiv \sqrt{z_{\rm UV}} \xi_L^-(z_{\rm UV})$.[19] The holographic Lagrangian for this system at the quadratic level is

$$\mathcal{L} = \bar{\psi}_R^- \frac{\not{p}}{p} \frac{\Pi_R}{z_{\rm UV}} \psi_R^- + \bar{\psi}_L^- \frac{\not{p}}{p} \frac{\Pi_L}{z_{\rm UV}} \psi_L^-, \tag{C4}$$

where $\Pi_L = -(\Pi_0 + \Pi_1/2)^{-1}$ and $\Pi_R = \Pi_0$, evaluated again with a Minkowski signature. The relevant on-shell field wave functions are

$$\begin{cases} \xi_R^-(z) = \frac{1}{\sqrt{z_{\rm UV}}} \left(\frac{z}{z_{\rm UV}}\right)^{5/2} \frac{G_{--}(c_u, -im_R, z_{\rm IR}, z)}{G_{--}(c_u, -im_R, z_{\rm IR}, z_{\rm UV})} \psi_R^- \equiv f_R^-(z) \psi_R^-, \\ \xi_L^-(z) = \frac{1}{\sqrt{z_{\rm UV}}} \left(\frac{z}{z_{\rm UV}}\right)^{5/2} \frac{G_{++}(c_u, -im_L, z_{\rm IR}, z)}{G_{++}(c_u, -im_L, z_{\rm IR}, z_{\rm UV})} \psi_L^- \equiv f_L^-(z) \psi_L^-. \end{cases} \tag{C5}$$

The normalization factors $Z^-_{L,R}$ can be found by expanding the action around the on-shell momentum. One gets[20]

$$(Z^-_{L,R})^2 = \lim_{p\to m_{L,R}} \frac{1}{2z_{\rm UV}} \frac{\Pi_{L,R}}{p - m_{L,R}} = \lim_{p\to m_{L,R}} \frac{1}{2z_{\rm UV}} \frac{\partial \Pi_{L,R}}{\partial p}, \tag{C6}$$

where $m_{L,R}$ are the masses of the NLOP.

The holographic description of the X_- gauge field is easily obtained in an axial-type gauge $X_{-,5} = 0$, as described in [61]. The quadratic holographic Lagrangian for the transverse part of the X_- gauge field is found to be

$$\mathcal{L} = -\frac{1}{2z_{\rm UV}} \hat{X}^t_{-,\mu} p \Pi_- \hat{X}^{t\mu}_-, \tag{C7}$$

where $\hat{X}^t_- \equiv \sqrt{z_{\rm UV}} X^t_-(z_{\rm UV})$ is the holographic field. The on-shell field wave function is

$$\begin{aligned} X^t_{-,\mu}(z) &= \frac{z}{z_{\rm UV}^{3/2}} \frac{G_{++}(1/2, -im_{X_-}, z_{\rm IR}, z)}{G_{++}(1/2, -im_{X_-}, z_{\rm IR}, z_{\rm UV})} \hat{X}^t_- \\ &\equiv f_{X_-}(z) \hat{X}^t_{-,\mu}, \end{aligned} \tag{C8}$$

and its normalization factor Z_{X_-} is

[18] The factor $1/z_{\rm UV}$ ensures that the holographic fields have canonical dimension in 4D.

[19] In the presence of EWSB, when the various field components are mixed by the Higgs VEV, it is better to choose holographic fields of the same chirality within a multiplet (see [61]). In the present case the two components are independent of each other, so we can simply use holographic fields with different chiralities.

[20] The factor $1/2$ which appears in these expressions is due to the fact that the fermions we are describing are massive. In the holographic approach the two chiralities of the fermions (say, $\phi_{L,R}$) are described by the same holographic field ($\hat{\phi}_L$), so that on shell $\phi_L = \hat{\phi}_L$ and $\phi_R = \not{p}/p \hat{\phi}_L$. In this case $\bar{\phi}(\not{p} - m)\phi \to \hat{\phi} 2(p - m)\not{p}/p \hat{\phi}_L$.

$$Z_{X_-}^2 = \lim_{p\to m_{X_-}} \frac{p}{z_{\rm UV}} \frac{\Pi_-}{p^2 - m_{X_-}^2} = \lim_{p\to m_{X_-}} \frac{\partial}{\partial p^2}\left(\frac{p\Pi_-}{z_{\rm UV}}\right). \tag{C9}$$

The interaction term can finally be written as

$$\begin{aligned}\mathcal{L}^{(3)} &= \frac{2}{3} g_{5X} \int_{z_{\rm UV}}^{z_{\rm IR}} dz \left(\frac{z_{\rm UV}}{z}\right)^4 (\bar{\xi}^-_{L/R} \not{X}_- \xi^+_{L/R} + \text{H.c.}) \\ &= \frac{2}{3} g_{5X} \bar{\psi}_{L/R} \not{\hat{X}}_- t_{L/R} \int_{z_{\rm UV}}^{z_{\rm IR}} dz \left(\frac{z_{\rm UV}}{z}\right)^4 (f^-_{L/R} f_{X_-} f^+_{L/R}) \\ &\quad + \text{H.c.},\end{aligned} \tag{C10}$$

where g_{5X} is the 5D $U(1)_X$ gauge coupling. Taking into account the normalization factors, we finally get

$$\tilde{g}_{L/R} = \frac{2}{3} \frac{g_{5X}}{Z^+_{L/R} Z^-_{L/R} Z_{X_-}} \int_{z_{\rm UV}}^{z_{\rm IR}} dz \left(\frac{z_{\rm UV}}{z}\right)^4 (f^-_{L/R} f_{X-} f^+_{L/R}). \tag{C11}$$

From the above relations it is possible to get an upper bound on $\tilde{g}_L$ and $\tilde{g}_R$ by noticing that both couplings are maximal when t_R and t_L reside mostly in the ξ_u multiplet, which occurs for $M_u \to \infty$ and $m_u \to \infty$, respectively.[21]

[21]Notice that in the limit $M_u \to \infty$, $m_u \to \infty$, the components of the ξ_u multiplet related to t_L and t_R acquire $(++)$ b.c., while the corresponding ξ_{q_1} components satisfy $(+-)$ boundary conditions [see also paragraph after Eq. (B11)].

When $M_u \to \infty$ and $c_u \simeq -1/2$, or $m_u \to \infty$ and $c_u \simeq 1/2$ one gets

$$\begin{aligned}&(Z_R^-)^2 \simeq (Z_L^-)^2 \simeq (Z_{X_-})^2, \qquad (Z_R^+)^2 \simeq \log(z_{\rm IR}/z_{\rm UV}), \\ &(Z_L^+)^2 \simeq m_u^2 \left(\frac{z_{\rm IR}}{z_{\rm UV}}\right)^{1-2c_{q_1}} \log(z_{\rm IR}/z_{\rm UV}), \\ &f_R^-(z) \simeq f_L^-(z) \simeq \left(\frac{z}{z_{\rm UV}}\right)^{3/2} f_{X_-}(z), \\ &f_R^+(z) \simeq \frac{1}{\sqrt{z_{\rm UV}}} \left(\frac{z}{z_{\rm UV}}\right)^{3/2}, \\ &f_L^+(z) \simeq -\frac{m_u}{\sqrt{z_{\rm UV}}} \left(\frac{z_{\rm IR}}{z_{\rm UV}}\right)^{1/2-c_{q_1}} \left(\frac{z}{z_{\rm UV}}\right)^{3/2}.\end{aligned} \tag{C12}$$

Using Eqs. (C12), we see that the integral over the wave functions in Eq. (C11) reduces to the normalization condition for the gauge field for both $\tilde{g}_R$ and $\tilde{g}_L$, giving simply

$$|\tilde{g}_{L/R}| \le \frac{2}{3} \frac{g_{5X}}{\sqrt{z_{\rm UV} \log(z_{\rm IR}/z_{\rm UV})}} = \frac{2}{3} g_X, \tag{C13}$$

where in the latter equality we have used the relation between the 5D coupling g_{5X} and the 4D coupling g_X. This proves Eq. (3.6) in the main text.

[1] L. Randall and R. Sundrum, Phys. Rev. Lett. **83**, 3370 (1999); **83**, 4690 (1999).
[2] Y. Grossman and M. Neubert, Phys. Lett. B **474**, 361 (2000); T. Gherghetta and A. Pomarol, Nucl. Phys. **B586**, 141 (2000); S. J. Huber and Q. Shafi, Phys. Lett. B **498**, 256 (2001).
[3] K. Agashe, A. Delgado, M. J. May, and R. Sundrum, J. High Energy Phys. 08 (2003) 050.
[4] K. Agashe, R. Contino, L. Da Rold, and A. Pomarol, Phys. Lett. B **641**, 62 (2006).
[5] R. Contino, Y. Nomura, and A. Pomarol, Nucl. Phys. **B671**, 148 (2003).
[6] K. Agashe, R. Contino, and A. Pomarol, Nucl. Phys. **B719**, 165 (2005).
[7] K. Agashe and R. Contino, Nucl. Phys. **B742**, 59 (2006).
[8] T. Appelquist, H. C. Cheng, and B. A. Dobrescu, Phys. Rev. D **64**, 035002 (2001).
[9] G. Panico, M. Serone, and A. Wulzer, Nucl. Phys. **B762**, 189 (2007).
[10] M. Regis, M. Serone, and P. Ullio, J. High Energy Phys. 03 (2007) 084.
[11] Y. Bai, arXiv:0801.1662.
[12] C. T. Hill and R. J. Hill, Phys. Rev. D **76**, 115014 (2007).
[13] J. M. Maldacena, Int. J. Theor. Phys. **38**, 1113 (1999); S. S. Gubser, I. R. Klebanov, and A. M. Polyakov, Phys. Lett. B **428**, 105 (1998); E. Witten, Adv. Theor. Math. Phys. **2**, 253 (1998).
[14] T. Hambye and M. H. G. Tytgat, Phys. Lett. B **659**, 651 (2008).
[15] H. C. Cheng and I. Low, J. High Energy Phys. 09 (2003) 051.
[16] G. Servant and T. M. P. Tait, Nucl. Phys. **B650**, 391 (2003).
[17] B. A. Dobrescu, D. Hooper, K. Kong, and R. Mahbubani, J. Cosmol. Astropart. Phys. 10 (2007) 012.
[18] K. Agashe and G. Servant, Phys. Rev. Lett. **93**, 231805 (2004); J. Cosmol. Astropart. Phys. 02 (2005) 002.
[19] K. Agashe, A. Falkowski, I. Low, and G. Servant, J. High Energy Phys. 04 (2008) 027.
[20] J. L. Diaz-Cruz, arXiv:0711.0488.
[21] F. Del Aguila and J. Santiago, J. High Energy Phys. 03 (2002) 010.
[22] M. S. Carena, E. Pontón, T. M. P. Tait, and C. E. M. Wagner, Phys. Rev. D **67**, 096006 (2003).
[23] M. Serone, in *IFAE 2005: 17th Italian Meeting on High Energy Physics*, edited by A. Tricomi, S. Albergo, and M.

Chiorboli, AIP Conf. Proc. No. 794 (AIP, New York, 2005), p. 139.
[24] G. von Gersdorff, N. Irges, and M. Quiros, arXiv:hep-ph/0206029.
[25] R. Contino, L. Da Rold, and A. Pomarol, Phys. Rev. D **75**, 055014 (2007).
[26] M. S. Carena, E. Pontón, J. Santiago, and C. E. M. Wagner, Phys. Rev. D **76**, 035006 (2007).
[27] A. D. Medina, N. R. Shah, and C. E. M. Wagner, Phys. Rev. D **76**, 095010 (2007).
[28] M. E. Peskin and T. Takeuchi, Phys. Rev. D **46**, 381 (1992).
[29] M. S. Carena, E. Pontón, J. Santiago, and C. E. M. Wagner, Nucl. Phys. **B759**, 202 (2006).
[30] Y. Sakamura and Y. Hosotani, Phys. Lett. B **645**, 442 (2007); Prog. Theor. Phys. **118**, 935 (2007).
[31] R. Barbieri, B. Bellazzini, V. S. Rychkov, and A. Varagnolo, Phys. Rev. D **76**, 115008 (2007).
[32] T. Lari *et al.*, arXiv:0801.1800.
[33] Z. Han and W. Skiba, Phys. Rev. D **71**, 075009 (2005).
[34] E. W. Kolb and M. S. Turner, Front. Phys. **69**, 1 (1990).
[35] E. Komatsu *et al.* (WMAP Collaboration), arXiv:0803.0547.
[36] K. Griest and D. Seckel, Phys. Rev. D **43**, 3191 (1991).
[37] G. Belanger, F. Boudjema, A. Pukhov and A. Semenov, Comput. Phys. Commun. **176**, 367 (2007).
[38] H. Baer, K. m. Cheung, and J. F. Gunion, Phys. Rev. D **59**, 075002 (1999).
[39] A. Sommerfeld, Ann. Phys. (Paris) **11**, 257 (1931); for a pedagogical derivation, see also L. D. Landau and F. M. Lifshitz, *Quantum Mechanics (Non-relativistic Theory)* (Pergamon Press, New York, 1977), 3rd ed., Sec. 136.
[40] J. Hisano, S. Matsumoto, M. Nagai, O. Saito, and M. Senami, Phys. Lett. B **646**, 34 (2007); M. Cirelli, A. Strumia, and M. Tamburini, Nucl. Phys. **B787**, 152 (2007).
[41] V. S. Fadin and V. A. Khoze, Yad. Fiz. **48**, 487 (1988) [Sov. J. Nucl. Phys. **48**, 309 (1988)].
[42] R. Barbieri and G. F. Giudice, Nucl. Phys. **B306**, 63 (1988).
[43] G. W. Anderson and D. J. Castano, Phys. Lett. B **347**, 300 (1995).
[44] S. J. Huber, C. A. Lee, and Q. Shafi, Phys. Lett. B **531**, 112 (2002).
[45] H. Davoudiasl, B. Lillie, and T. G. Rizzo, J. High Energy Phys. 08 (2006) 042.
[46] M. S. Carena, A. Delgado, E. Pontón, T. M. P. Tait, and C. E. M. Wagner, Phys. Rev. D **68**, 035010 (2003).
[47] C. Csaki, C. Grojean, H. Murayama, L. Pilo, and J. Terning, Phys. Rev. D **69**, 055006 (2004).
[48] G. Cacciapaglia, C. Csaki, G. Marandella, and J. Terning, Phys. Rev. D **75**, 015003 (2007).
[49] R. Sekhar Chivukula, B. Coleppa, S. Di Chiara, E. H. Simmons, H. J. He, M. Kurachi, and M. Tanabashi, Phys. Rev. D **74**, 075011 (2006); R. Sekhar Chivukula, E. H. Simmons, S. Matsuzaki, and M. Tanabashi, Phys. Rev. D **75**, 075012 (2007).
[50] G. Cacciapaglia, C. Csaki, C. Grojean, and J. Terning, Phys. Rev. D **71**, 035015 (2005).
[51] R. Bonciani, S. Catani, M. L. Mangano, and P. Nason, Nucl. Phys. **B529**, 424 (1998).
[52] R. Contino and G. Servant, arXiv:0801.1679.
[53] K. Agashe, A. Belyaev, T. Krupovnickas, G. Perez, and J. Virzi, Phys. Rev. D **77**, 015003 (2008); B. Lillie, L. Randall, and L. T. Wang, J. High Energy Phys. 09 (2007) 074; B. Lillie, J. Shu, and T. M. P. Tait, Phys. Rev. D **76**, 115016 (2007); A. Djouadi, G. Moreau, and R. K. Singh, Nucl. Phys. **B797**, 1 (2008); K. Agashe *et al.*, Phys. Rev. D **76**, 115015 (2007); M. Carena, A. D. Medina, B. Panes, N. R. Shah, and C. E. M. Wagner, Phys. Rev. D **77**, 076003 (2008).
[54] H. C. Cheng, J. L. Feng, and K. T. Matchev, Phys. Rev. Lett. **89**, 211301 (2002).
[55] M. Drees and M. Nojiri, Phys. Rev. D **48**, 3483 (1993).
[56] M. A. Shifman, A. I. Vainshtein, and V. I. Zakharov, Phys. Lett. **78B**, 443 (1978).
[57] D. S. Akerib *et al.*, Nucl. Instrum. Methods Phys. Res., Sect. A **559**, 411 (2006).
[58] C. A. Scrucca and M. Serone, Int. J. Mod. Phys. A **19**, 2579 (2004).
[59] T. Hirayama and K. Yoshioka, J. High Energy Phys. 01 (2004) 032.
[60] T. Aaltonen *et al.* (CDF Collaboration), Phys. Rev. Lett. **100**, 161803 (2008).
[61] G. Panico and A. Wulzer, J. High Energy Phys. 05 (2007) 060.
[62] M. A. Luty, M. Porrati, and R. Rattazzi, J. High Energy Phys. 09 (2003) 029; R. Barbieri, A. Pomarol, and R. Rattazzi, Phys. Lett. B **591**, 141 (2004); R. Contino and A. Pomarol, J. High Energy Phys. 11 (2004) 058.